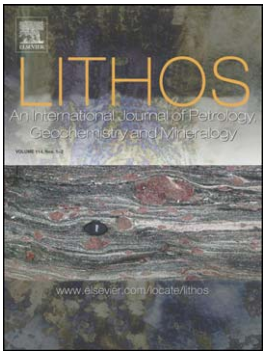

Fractionation of Li, Be, Ga, Nb, Ta, In, Sn, Sb, W and Bi in the peraluminous Early Permian Variscan granites of the Cornubian Batholith: precursor processes to magmatic-hydrothermal mineralisation

Beth Simons, Jens C.Ø. Andersen, Robin K. Shail, Frances Jenner

PII: S0024-4937(17)30050-6
DOI: doi:10.1016/j.lithos.2017.02.007
Reference: LITHOS 4233

To appear in: *LITHOS*

Received date: 9 November 2016
Accepted date: 8 February 2017

Please cite this article as: Simons, Beth, Andersen, Jens C.Ø., Shail, Robin K., Jenner, Frances, Fractionation of Li, Be, Ga, Nb, Ta, In, Sn, Sb, W and Bi in the peraluminous Early Permian Variscan granites of the Cornubian Batholith: precursor processes to magmatic-hydrothermal mineralisation, *LITHOS* (2017), doi:10.1016/j.lithos.2017.02.007

Fractionation of Li, Be, Ga, Nb, Ta, In, Sn, Sb, W and Bi in the peraluminous Early Permian Variscan granites of the Cornubian Batholith: precursor processes to magmatic-hydrothermal mineralisation.

Beth Simons[1*], Jens C.Ø. Andersen[1], Robin K. Shail[1], Frances Jenner[2]

[1]Camborne School of Mines, College of Engineering, Mathematics and Physical Sciences, University of Exeter, Penryn Campus, Cornwall, United Kingdom, TR10 9FE.

[2]The Open University, School of Environment, Earth & Ecosystems, Milton Keynes, United Kingdom, MK7 6AA.

*Corresponding author email: B.Simons@exeter.ac.uk

Keywords: granite; geochemistry; trace metals; Variscan; peraluminous; Cornubian

ABSTRACT

The Early Permian Variscan Cornubian Batholith is a peraluminous, composite pluton intruded into Devonian and Carboniferous metamorphosed sedimentary and volcanic rocks. Within the batholith there are: G1 (two-mica), G2 (muscovite), G3 (biotite), G4 (tourmaline) and G5 (topaz) granites. G1-G2 and G3-G4 are derived from greywacke sources and linked through fractionation of assemblages dominated by feldspars and biotite, with minor mantle involvement in G3. G5 formed though flux-induced biotite-dominate melting in the lower crust during granulite facies metamorphism. Fractionation enriched G2 granites in Li (average 315 ppm), Be (12 ppm), Ta (4.4 ppm), In (74 ppb), Sn (18 ppm) and W (12 ppm) relative to crustal abundances and G1 granites. Gallium (24 ppm), Nb (16 ppm) and Bi (0.46 ppm) are not significantly enriched during fractionation, implying they are more compatible in the fractionating assemblage. Sb (0.16 ppm) is depleted in G1-G2 relative to the average upper and lower continental crust. Muscovite, a late-stage magmatic/subsolidus mineral, is the major host of Li, Nb, In, Sn and W in G2 granites. G2 granites are spatially associated with W-Sn greisen mineralisation.

Fractionation within the younger G3-G4 granite system enriched Li (average 364 ppm), Ga (28 ppm), In (80 ppb), Sn (14 ppm), Nb (27 ppm), Ta (4.6 ppm), W (6.3 ppm) and Bi (0.61 ppm) in the G4 granites with retention of Be in G3 granites due to partitioning of Be into cordierite during fractionation. The distribution of Nb and Ta is controlled by accessory phases such as rutile within the G4 granites, facilitated by high F and lowering the melt temperature, leading to disseminated Nb and Ta mineralisation. Lithium, In, Sn and W are hosted in biotite micas which may prove favourable for breakdown on ingress of hydrothermal fluids. Higher degrees of scattering on trace element plots may be attributable to fluid-rock interactions or variability within the magma chamber. The G3-G4 system is more boron-rich, evidenced by a higher modal abundance of tourmaline. In this system, there is a stronger increase of Sn compared to G1-G2 granites, implying Sn in tourmaline-dominated mineral lodes may represent exsolution from G4 granites.

G1-G4 granite abundances can be accounted for by 20-30% partial melting and 10-40% fractionation of a greywacke source. G5 granites are analogues of Rare Metal Granites described in

France and Germany. These granites are enriched in Li (average 1363 ppm), Ga (38 ppm), Sn (21 ppm), W (24 ppm), Nb (52 ppm) and Ta (15 ppm). Within G5 granites, the metals partition into accessory minerals such as rutile, columbite-tantalite and cassiterite, forming disseminated magmatic mineralisation. High observed concentrations of Li, In, Sn, W, Nb and Ta in G4 and G5 granites are likely facilitated by high F, Li and P, which lower melt temperature and promote retention of these elements in the melt, prior to crystallisation of disseminated magmatic mineralisation.

1. INTRODUCTION

Growth in the low carbon and consumer electronics sectors has led to a rise in demand for metals that are not typical historical exploration and mining targets. For instance, indium (In), beryllium (Be) and bismuth (Bi) are used extensively in products such as solar panels and touch screen devices, and lithium (Li) is essential for high capacity energy storage (Moss et al., 2011). Several metals including Be, niobium (Nb), tantalum (Ta), antimony (Sb), gallium (Ga), tungsten (W) and bismuth (Bi) are identified as having strategic importance for the UK and the EU (e.g. House of Commons, 2011; European Commision, 2014). Consumption of several of these metals already outstrips supply and there is an immediate need to identify further resources. In addition, market price fluctuations in some major metals such as Zn can impact the supply of minor 'speciality' metals that are produced solely as by-products, particularly In, for which sphalerite is a major carrier (e.g. Cook et al., 2009; Jovic et al., 2011)

Peraluminous granites are a major global source of magmatic and magmatic-hydrothermal ore deposits, particularly for elements often described as lithophile during the petrogenesis of granitic melts (Li, Nb, Ta, Be, Sn and W) (e.g. Černý et al., 2005; Sial et al., 2011). Factors such as source composition (Romer and Kroner, 2014), degree of fractionation (Lehmann, 1987; Taylor and Wall, 1992) and hydrothermal overprinting (Štemprok, 1987; Haapala, 1997) control enrichment of these lithophile metals within granites. There are limited studies on the behaviour of Ga, In, W and Bi during source melting and fractionation of peraluminous granite magmas. A prerequisite for understanding the distribution of rare metals in magmatic-hydrothermal systems is an understanding

of their behaviour in precursor magmas prior to, and during, the exsolution of magmatic-hydrothermal fluids.

The purpose of this study is to further understanding of the magmatic behaviour of Li, Be, Ga, Nb, Ta, In, Sn, W, Sb and Bi in peraluminous granitic systems through an investigation of the Variscan granites of the Cornubian Batholith in SW England. The region has an extensive history of mining. It has historical and contemporary production of metals now deemed "critical" (e.g. Bi, W, Sb) and there is evidence for In concentrations comparable to those in regions of China and Canada (e.g. Jackson et al., 1989; Cook et al., 2011a; Andersen et al., 2016). There are several stages of (largely) fracture-controlled mineralisation related to the release of magmatic-hydrothermal fluids during, and immediately after pluton construction, with variable mixing between meteoric and metamorphic fluids (e.g. Jackson et al., 1989). Mineralisation styles are diverse, and granite-related mineralisation encompasses magnetite and sulphide skarns with silicate-hosted Sn, greisen-bordered sheeted vein complexes (W-Sn), quartz-tourmaline veins and breccias (Sn) and polymetallic sulphide lodes (Cu, Zn, As, Sn); Scrivener (2006) and references therein. A previous study indicates that evolved tourmaline-bearing granites are enriched in metals such as Sn and are a likely magmatic precursor to mineralisation in the region (Müller et al., 2006).

In this study, we present geochemical data for the occurrence of Li, Be, Ga, Nb, Ta, In, Sn, Sb, W and Bi within the variably evolved early Permian granites of the lower plate, post-collisional, peraluminous Cornubian Batholith. In so doing, we are able to evaluate metal behaviour during the evolution of peraluminous magmas. We explore the distribution of these elements within major silicate minerals and discuss the implications for metal partitioning and metallogeny. Finally, we evaluate the processes, using geochemical modelling, that control the distribution of the metals during evolution of the Cornubian Batholith and discuss how these constraints can be used to assess potential rare metal enrichment elsewhere, particularly within the European Variscides.

2. GEOLOGICAL SETTING

2.1. Regional tectonic evolution

The Variscan belt stretches across Western Europe and represents the collision between Laurussia, Gondwana and several peri-Gondwana microplates from the Devonian to the Carboniferous (Stampfli et al., 2013). South west England lies within the Rhenohercynian Zone, representing a short-lived marginal or successor basin that formed during or after the closure of the Rheic Ocean (Franke, 2000). In the Early Devonian, the region underwent rifting and passive margin development, with deposition of shallow marine sandstones, siltstones and mudstones and rift-related basaltic lavas and gabbros in E-W trending sedimentary graben and half-graben structures (Floyd et al., 1991; Leveridge and Hartley, 2006). During Late Devonian convergence, SW England occupied a lower plate position, with continental collision initiating in the early Carboniferous (Shail and Leveridge, 2009). Metamorphism of the Devonian-Carboniferous basin successions is very low grade (epizone-anchizone), with localised greenschist facies in Devonian rocks (Warr et al., 1991). By the late Carboniferous (c. 305 Ma), Variscan convergence had been replaced by a dextral transtensional regime, with reactivation of Variscan thrusts and development of new fault systems during NNW-SSE lithospheric extension continuing throughout most of the Early Permian (Alexander and Shail, 1995). Red-bed sedimentary successions were deposited and mantle-derived lamprophyres and high-K basalts erupted and intruded during this Early Permian extension (e.g. Leat et al., 1987; Shail and Wilkinson, 1994; Dupuis et al., 2015) The lamprophyres and basalts are contemporaneous with the main expression of post-collisional magmatism represented by the Cornubian Batholith (Dupuis et al., 2015).

2.2. The Cornubian Batholith

The Cornubian Batholith is a WSW-ENE trending, 250 km long and 20-40 km wide composite granite intrusion extending from beyond the Isles of Scilly in the west to Dartmoor in the east, at the current erosional level. The batholith is hosted by a passive margin succession of Devonian and Carboniferous sedimentary and volcanic rocks (Willis-Richards and Jackson, 1989; Shail and Leveridge, 2009). The two-mica (G1) and muscovite (G2) granites represent the oldest magmatism in the region with U-Pb monazite ages from 293.7 ± 0.6 to 281.7 ± 0.8 Ma (Chesley et al., 1993; Clark et al., 1994). The former are confined to the Isles of Scilly, Carnmenellis and Bodmin

plutons with minor G2 granite stocks at Carn Marth, Cligga, Kit Hill and Hemerdon. Biotite (G3) granites represent a significant second stage of magmatic activity in SW England, with U-Pb monazite ages from 281.8 ± 0.8 to 272.3 ±1.8 Ma (Chen et al., 1993; Chesley et al., 1993) and are confined to the Land's End, St. Austell and Dartmoor plutons (Fig. 1). Associated with G3 granites are evolved tourmaline (G4) granites, forming dykes and small stocks within the Land's End, St. Austell and Dartmoor plutons. Topaz (G5) granites and aplites form small stocks within the St. Austell Granite and comprise the majority of the Tregonning Granite, the latter of which has an Ar-Ar zinnwaldite cooling age of 281.0 ± 1.3 Ma (Clark et al., 1994). Across the batholith there are minor aplites and pegmatites associated with G1-G5 granites (e.g. Dangerfield and Hawkes, 1981; Manning et al., 1996; Müller et al., 2006; Simons et al., 2016) (Fig. 1). Other expressions of magmatism include rhyolite/microgranite dykes, locally termed "elvans" and rhyolitic lavas, which are now extensively exposed as clasts in Permian red-bed sediments.

2.2.1. Two-mica (G1) and muscovite (G2) granites

The G1 granites are coarse- (G1a) to fine-grained (G1c), commonly porphyritic, and are mainly monzogranites. They have perthitic orthoclase phenocrysts (<25 mm), 5-10 modal % trioctahedral micas (Mg siderophyllite / siderophyllite), up to 6 modal % muscovite, 1 modal % tourmaline and a variety of accessory minerals including zircon, monazite, xenotime, andalusite, apatite, ilmenite, fluorite and topaz (Fig. 2a). Enclaves of granites within each other, metasedimentary enclaves and strained quartz are widespread throughout all G1 (Fig. 2b) (Exley and Stone, 1964; Charoy, 1986; Chappell and Hine, 2006; Simons et al., 2016).

Muscovite (G2) granites are confined to small stocks such as Cligga, Kit Hill and Hemerdon. G2 granites are fine- to coarse-grained with variable sizes and abundances of perthitic orthoclase phenocrysts. Muscovite is dominant, up to 10 modal %, with trioctahedral micas, which are Li siderophyllite, trending towards zinnwaldite in composition. Plagioclase trends towards near albite compositions and tourmaline reaches up to 2 modal %. Accessory minerals include topaz, apatite, zircon, rutile (Nb-bearing) and fluorite. The muscovite granites are spatially associated with W-Sn greisen-bordered veins (Fig. 2c) (Exley and Stone, 1964). The G1 and G2 granites are linked through

fractionation of an assemblage dominated by biotite, feldspars, zircon, monazite, allanite and apatite. They are derived from a greywacke-type source within the lower crust, with melting at moderate temperatures (731-806°C) and pressures (>5 kbar) (Charoy, 1986; Chappell and Hine, 2006; Simons et al., 2016).

2.2.2. Biotite (G3) and tourmaline (G4) granites

The G3 granites are coarse- (G3a) to fine-grained (G3d), commonly porphyritic, and are mainly monzogranites. They have perthitic orthoclase phenocrysts (>25 mm), 10 modal % trioctahedral micas (Mg siderophyllite / siderophyllite), up to 2.5 modal % tourmaline and a variety of accessory minerals including cordierite, muscovite, zircon, monazite, xenotime, andalusite, apatite, ilmenite, and fluorite (Fig. 2d).

Tourmaline (G4) granites are texturally variable, comprising fine-grained (G4a), globular quartz (G4b) and coarse-grained Li mica-bearing porphyritic variants (G4c) (Fig. 2e) (Manning et al., 1996). G4 granites are spatially associated with G3 granites, for example, forming gradational contacts, and are therefore confined to the Land's End, St. Austell and Dartmoor plutons. In G4 granites, tourmaline is the dominant ferromagnesian mineral, with Li-rich trioctahedral micas (Li siderophyllite, zinnwaldite) and approximately equal abundances of orthoclase and albite ($An_{<8}$). Accessory minerals include muscovite, topaz, cordierite, apatite, zircon, monazite, Nb-(Ta)-rutile, phosphates and fluorite (Hill and Manning, 1987; Manning et al., 1996). Metasedimentary and mafic microgranular enclaves (MME), along with quartz-tourmaline orbicules and pegmatitic pockets are widespread throughout all G3 and G4 granites (Fig. 2f; Stimac et al., 1995; Müller et al., 2006; Drivenes et al., 2015).

The G3 and G4 granites appear to be linked through fractionation of an assemblage dominated by biotite and feldspars with minor zircon, monazite, allanite and apatite. They are derived from a greywacke-type source within the lower crust, with melting at higher temperatures (768-847°C) and lower pressures (<5 kbar) than G1-G2 granites, due to continued intrusion of mafic igneous rocks into the crust during ongoing extensional and erosional exhumation of the lower plate. There is a minor mantle component in the G3 granites and scatter on major element plots is

interpreted as evidence for fluid overprint (Darbyshire and Shepherd, 1994; Simons et al., 2016), although this may represent variable pulses of evolved melt from a deep magma chamber (e.g. Merino et al., 2013).

2.1.3. Topaz (G5) granites

The topaz (G5a) granites are medium-grained, equigranular and aphyric and distinguished by up to 3 modal % of euhedral to subhedral topaz and Li-Fe trioctahedral micas such as zinnwaldite and lepidolite (Fig. 2g) (Stone et al., 1988; Henderson et al., 1989). The Tregonning Granite and Nanpean and Hensbarrow stocks within the St. Austell Granite are the main exposures. Contacts with adjacent G3 and G4 granites from now inaccessible exposures within the St Austell Granite are reported to be sharp, with zones of pegmatite and aplite and localised zones of extensive tourmalinisation developed in host granite or metasedimentary rock (Manning and Hill, 1990). Topaz-rich aplite (G5b) and pegmatite sheets are associated with the Tregonning Granite, where they primarily occur in metasedimentary host rocks. The Meldon Aplite, north of the Dartmoor Granite, is a topaz aplite, but there is no outcrop of G5 granite. Accessory minerals are diverse, comprising apatite, amblygonite, zircon Nb-(Ta)-rutile, Mn-ilmenite, columbite-tantalite and cassiterite (Stone and George, 1978; Scott et al., 1998). The topaz granites do not appear to be petrogenetically linked to the G1-G2 or G3-G4 granites and are interpreted as forming from fluid-fluxed melting of a biotite-rich source, with the fluids derived from granulite facies metamorphism in the lower crust (Stone, 1992; Simons et al., 2016).

3. METHODOLOGY

Granite samples (n=91) were primarily those described by Simons et al. (2016); additional samples used by Müller et al. (2006) were obtained from the Natural History Museum, London (collection BM.2004,P14, specimen numbers 1, 7, 8, 10, 21, 23, 24, 30 and 31). Lamprophyre (n=9) and basalt (n=3) samples were collected from across SW England to provide a mantle end-member composition required to assess the potential for mixing of mantle and felsic melts. Mafic

microgranular enclave samples (n=2) from some of the locations studied by Stimac et al. (1995) were also analysed.

Major elements, Ga, Nb and Sn were determined by X-ray fluorescence (XRF) analysis at Activation Laboratories, Canada. Samples were prepared as fused beads for major elements and pressed powder pellets for Ga, Nb and Sn. Major element data with standard reference material (SRM) recoveries are reported by Simons et al. (2016). The remaining trace elements (Li, Be, In, Sb, W, Bi) were determined following the methods of Yu et al. (2001) using an Agilent 7700 ICP-MS at Camborne School of Mines, along with Ga, Nb and Sn for validation purposes. Prior to analysis, the instrument was calibrated using multi-elemental standard solutions and sampling depth and carrier gas flow were tuned to ensure that oxide and doubly charged ion formation were kept <1%. Isotope ^{115}In (95.7% of naturally occurring In) has an isobaric interference with ^{115}Sn (0.34% of naturally occurring Sn). This isobaric interference was corrected by monitoring ^{118}Sn (24.22% of naturally occurring Sn, interference free), and subtracting the corresponding signal from ^{115}In that represents ^{115}Sn (see also White et al., 2015). Detection limits were estimated at 10 times the standard deviation of 10 blanks (typically <0.5 ppm). The analytical reproducibility is generally better than 10%, except for Sb which is 12%. International standard reference material (GSP-2, BCR-1) and internal standards show excellent agreement with certified and preferred (Sn, In, W, Bi, Sb) values (Supplementary Table 1).

Polished petrographic thin sections were prepared at Camborne School of Mines. Electron–probe microanalysis (EPMA) of micas, feldspars, topaz, tourmaline and cordierite was carried out on a JEOL JXA-8200 superprobe with four wavelength dispersive detectors. Two of the detectors have a high count rate suitable for analysis of trace elements. For EPMA analysis, a 10 μm spot was used to minimise loss of F and Na with an accelerating voltage of 15 kV and charge of 1.5 x 10^{-8} A. Data reduction followed the ZAF method. Calibration was checked using a secondary standard (Astimex Biotite) that contained the elements in a similar proportion to those expected in the unknown samples. Chemical analyses were converted to the empirical formulae on the basis of the appropriate number of atoms of oxygen in a formula unit (apfu).

Eight selected samples were prepared as 100 μm thick polished thin sections. The samples chosen contained a range of trioctahedral (biotite group) mica and plagioclase compositions along

with topaz and cordierite in a range of mineral assemblages and granite types. Laser-ablation inductively coupled spectroscopy (LA-ICP-MS) analysis was carried out over three consecutive days using an Agilent 7500 quadrupole ICP-MS with a New Wave 213 laser system at the Open University, Milton Keynes, UK. Samples were ablated using a laser spot diameter of 100 μm and a repetition rate of 18 Hz with 70s of analysis time (30s background, 40s ablation). The ICP-MS was tuned prior to analysis to ensure low oxide and doubly charged ion production rates. Elements analysed included: ^{7}Li, ^{27}Al, ^{29}Si, ^{43}Ca, ^{49}Ti, ^{57}Fe, ^{69}Ga, ^{71}Ga, ^{93}Nb, ^{115}In, ^{118}Sn, ^{181}Ta and ^{182}W, following the methods described in Jenner and O'Neill (2012), and using silica content determined by EPMA for internal calibration of analyses. Precision is better than 5% for most elements, with the exception of Ti (10%) and Fe (13%). Analyses of the unknown minerals were collected in batches of 12 with NIST 612 and BCR-2G used for external calibration, using values and given by Jenner and O'Neill (2012) (Supplementary Table 2).

4. RESULTS

4.1. Whole-rock geochemistry

It is well established that the granites of the Cornubian Batholith are peraluminous, with A/CNK [(Al_2O_3/($CaO+N_2O+K_2O$)] values of >1.2 and average SiO_2 contents >70 wt.% (e.g. Darbyshire and Shepherd, 1985; Charoy, 1986; Manning et al., 1996; Chappell and Hine, 2006; Müller et al., 2006). Two-mica (G1) and biotite (G3) granites have the lowest average SiO_2 (70-72 wt.%) and higher abundances of Ti, Fe, Mg and Ca relative to the more evolved muscovite (G2) and tourmaline (G4) granites. Barium, Sr, Pb, Th, U, Zr and the REE are lower and Rb higher in the geochemically evolved G2 and G4 granites, which also have stronger Eu anomalies, respectively, relative to the G1 and G3 granites (Chappell and Hine, 2006; Müller et al., 2006; Simons et al., 2016). Topaz (G5) granites have SiO_2 contents of 71-72 wt.%, lower Ti, Mg, Fe, REE, Th, U and Zr with higher Al, Rb, and P abundances relative to the G1-G4 granites (Stone, 1975, 1992). The Cornubian granites are enriched in elements such as As, B, Cl, F, Pb, Rb, U and Zn relative to peraluminous granites elsewhere in the world (Willis-Richards and Jackson, 1989).

Relative to the average upper (UCC) and lower (LCC) continental crust abundances of Rudnick and Gao (2004) and the crustal abundances of Hu and Gao (2008), the Cornubian Batholith shows strong enrichment in Li (and associated Rb, F enrichment) with moderate enrichment in Be, Sn, Ta, W and Bi. Antimony is higher in all continental crust estimates relative to the Cornubian Batholith, whereas Ga, In and Nb are broadly similar. Metasedimentary rocks of the region, which can be regarded as a proxy for a granite source (e.g. Simons *et al*., 2016) show a slight enrichment of Li relative to upper and lower crustal values, with Sn and Nb comparable to lower crustal abundances (Hall, 1990) (Table 1, Fig. 3). On UCC-normalised multi-element plots, the less evolved G1 and G3 granites are characterised by lower abundances of all rare metals, with the exception of Sb. Evolved G2 granites are enriched in Be and W relative to the less evolved G1 granites, whereas these elements decrease and remain constant respectively for G4, relative to the less evolved G3 granites. G5 granites show significantly enriched abundances of Li, Nb, Ta and W compared to the G1, G2, G3 and G4 granites (Fig. 3).

Using $1/TiO_2$ as a fractionation indicator, where increasing $1/TiO_2$ indicates increasing degrees of fractionation or a variable source (e.g. Förster et al., 1999; Romer et al., 2014), the metals show differing behaviour across the G1-G2, G3-G4 and G5 granites (Fig. 4). Niobium and Ta increase with granite fractionation with stronger increases for Nb in G3-G4 granites. Li and Ga are significantly elevated in the G3-G4 granite series relative to G1-G2 granites. Conversely, In, Sn, W and Bi increase in G1-G2 granites, but within the G3-G4 series, several G4 values scatter towards lower In, Sn and Bi abundances, with no strong trend for W in G3-G4 granites. Beryllium shows increases with fractionation in G1-G2 granites, but decreases in G3-G4 granites. Antimony shows no overall trends with variations in $1/TiO_2$. Limited data from the G5 granites (n=9) means that no clear trends are discernible, but these granites invariably plot towards extremes of all values, except for Be, In, Sb and Bi compared to the G1, G2, G3 and G4 granites.

Regional maps displaying the distribution of Li, Be, Ga, Nb, Ta, In, Sn, Sb, W and Bi identify variations in the behaviour of these metals within the magmatic system (Fig. 5). There are clear increases in abundance with granite fractionation for Li, Ga, Nb, Ta and Sn, with the highest abundances of these metals confined to geochemically evolved G2 and G4 granites (Fig. 5c-e,g).

Lithium is particularly enriched in the lepidolite-bearing Tregonning Granite and Meldon Aplite, both with abundances in the 99th percentile. These localities are also enriched in Ga, Nb, Ta and W. Indium, which generally shows an enrichment in G2 and G4 granites, shows higher average abundances in the Land's End Granite and within the Carnmenellis Granite, regardless of the granite type (Fig. 5f). Beryllium is unique in showing a marked increase in medium-grained G1b (Fig. 1) and G2 granites, but not in G4 granites, indicated by abundances in the 98th percentile upwards within the Cligga, Carn Marth and Kit Hill G2 granites (Fig. 5b). The behaviour of Sb isn't related to the degree magmatic evolution, with high abundances centred in locations such as Burras (Carnmenellis), Hemerdon, Lamorna (Land's End) and Yes Tor (Dartmoor) that have no petrogenetic links (Fig. 5h). It is also apparent from these maps, that Sn and W have a decoupled relationship, with the former more strongly enriched in the younger, boron-rich systems of the G3-G4 granites than the latter.

4.2. Mineral chemistry

There are very limited data on the partitioning of metals such as In, Sn and W within major silicate minerals in peraluminous granites. Previous studies suggest that muscovite is the dominant host of Sn and W over biotite (Alderton and Moore, 1981; Neiva et al., 2002) and that biotite may contain In (Miroshnichenko, 1965). Incorporation of trace elements, with variable ionic radii and charge, into micas is well established (Tischendorf et al., 2001 and references therein). Tourmaline can also incorporate such elements including Sn and W (Marks et al., 2013). Niobium and Ta are known to be incorporated into rutile in G3, G4 and G5 granites and associated mineralisation (Scott et al., 1998; Müller and Halls, 2005; Drivenes et al., 2015) and can also partition into biotite and white mica (Stepanov et al., 2014).

The trioctahedral (biotite group) micas reflect granite evolution. G1 and G3 granites have Mg siderophyllite or siderophyllite as the trioctahedral mica composition, with a continuum, represented by increasing Li and decreasing Mg through Li siderophyllite in G2 granites and zinnwaldite in G4 granites (Stone et al., 1988; Henderson et al., 1989; Müller et al., 2006). Muscovite has two forms, with primary euhedral muscovite closer to true muscovite compositions and late-stage muscovite, containing increased Li and/or Fe, trending towards ferroan muscovite or lithian ferroan muscovite

compositions (Simons et al., 2016). Plagioclase compositions evolve from oligoclase in G1/G3 granites through to albite in G2/G4 granites, whereas alkali feldspar is orthoclase-perthite in all granite types (Müller et al., 2006; Simons et al., 2016). Tourmaline is primarily schorl, with increased Li and decreased Mg and Fe in G2/G4 granites, occasionally reaching elbaite composition in G5 granites (London and Manning, 1995; Drivenes et al., 2015). The samples analysed by LA-ICP-MS, representative of the different mineralogical association across the batholith, are detailed in Table 2.

4.2.1. G1-G2 granite

Trioctahedral micas are the dominant hosts of Li within G1 and G2 granites with average Li abundances ranging from (average) 3097 ppm in Mg siderophyllite to 6070 ppm in Li siderophyllite. Primary muscovite hosts minor Li (average 1250 ppm), as does late-stage ferroan muscovite (1547 ppm) (Table 3). Gallium is distributed fairly evenly across mica and tourmaline (average 95-157 ppm), with minor amounts in feldspars (21-34 ppm). The majority of the Nb and Ta are incorporated into muscovite and biotite micas in G1 granites. Within G2 granites, whilst much of the Nb is incorporated in micas, the bulk of the Ta (69%) resides in an unknown mineral (Fig. 6a-c), most likely a Fe-Ti oxide. Indium and W are dominantly hosted by muscovite in G2 granites with average abundances of 0.74 ppm and 124 ppm respectively. Tin has maximum average abundance of 63 ppm in muscovite, but is also incorporated in minor (<20 ppm) amounts in plagioclase (albite), perthitic orthoclase and tourmaline.

4.2.2. G3-G4 granite

Trioctahedral micas show strong enrichment in Li within G3-G4 granites, averaging 3247 in siderophyllite and 16299 ppm in zinnwaldite. Cordierite is also a major host of Li within G3 granites, with an average abundance of 3857 ppm. The majority of the whole rock Li budget is accounted for by trioctahedral micas in both G3 and G4 granites. As with G1-G2 granites, Ga is distributed evenly across plagioclase, micas, perthitic orthoclase and tourmaline (Fig. 6d-e). Niobium and Ta are primarily hosted in trioctahedral mica in G3 granites but over 80% of the whole rock abundance in G4 granites is accounted for by accessory minerals, most likely Fe-Ti oxides. Indium and Sn are hosted

within micas and have higher average abundances in G4 granite zinnwaldite, 1.11 and 111 ppm respectively, than micas within G1-G2 granites. Tungsten has an average abundance of 163 ppm in zinnwaldite in G4 granites and partitions into an unknown mineral in G3 granites (Table 3).

4.2.3. G5 granite

Near ideal composition lepidolite micas are the major host of Li within G5 granites, with an average abundance of 22650 ppm (4.88 wt.%). Gallium, as with G1-G4 granites, is distributed evenly between all major silicates (Fig. 6f). Abundances of Nb, Ta, In and Sn are lower in mica and feldspars than for G1-G4 granites, with the distribution of these metals, particularly Nb and Ta, controlled by a trace or accessory mineral. Tungsten has high average abundances (195 ppm), but also partitions into an accessory mineral. Topaz is not a dominant host of any rare metal, with only Ga having an average abundance above 2 ppm (Table 3).

Across all of the granite types, abundances of Sn and W in micas are consistent with the studies by Neves (1997) and Gomes and Neiva (2002); in both of these studies biotite is the primary host of Sn. Tourmaline from Schwarzwald, Germany, has lower abundances of Li, but similar Nb, Ta, Sn and W (Marks et al., 2013). Topaz in SW England remains unenriched in Sn-W and rare metals, converse to findings in the Erzgebirge, where topaz contains 5-35 ppm Ga and up to 23 ppm Sn (Breiter et al., 2013)

6. TRACE ELEMENT MODELLING

6.1. Methods

The G1-G2 and G3-G4 granites are predominantly crustally-sourced, with a very minor contribution (<10%) from mantle-derived melts within the G3-G4 granites (Charoy, 1986; Darbyshire and Shepherd, 1994; Chappell and Hine, 2006; Simons et al., 2016). Lower crustal source rocks are not exposed in SW England, so fur samples of Gramscatho Group metagreywacke, used in the studies of Floyd et al. (1991) and Darbyshire and Shepherd (1994), have been used as a compositional proxy and were analysed for their rare metal contents (Table 1). Although these metagreywackes were

derived from the upper plate during Variscan convergence, their T^{DM} model ages are similar to those for the granites and suggest that their lower plate source shared a similar peri-Gondwanan basement origin (Shail and Leveridge, 2009; Nance et al., 2015). The rare metal abundances of greywacke from Hu and Gao (2008) are also utilised as a proxy composition and these are very similar to geochemical analyses of the Gramscatho Group greywackes.

There are limited experimentally determined partition coefficients for the metals in this study. For geochemical modelling of source melting and fractional crystallisation, partition coefficients for Li, Be, Ga, Nb and Ta in peraluminous granites are taken from the literature (Table A.1). The partition coefficients for In, Sn, Sb , W and Bi in biotite and garnet in a basanite (Adam and Green, 2006) indicate incompatible behaviour of these elements during melting, with the exception of In, which displays compatibility in garnet (garnet/melt = 10.3 ± 9.3 to 87 ± 50, Adam and Green, 2006). Approximations of mineral/melt partition coefficients using phenocryst/matrix measurements indicate that biotite and muscovite host Sn and W (i.e. $D^{mineral/melt} > 1$), whereas feldspar and quartz can host Sn and W, but with $D^{mineral/melt}$ typically <1 (e.g. Lehmann, 1990); quartz from rare metal granite (RMG) pegmatites contains less than 1 ppm Sn (Breiter, 2014). This is consistent with the findings of this study; mineral/melt ratios of Sn and W in micas are >1 and <1 for feldspars (Appendix, Table A.1.), implying that fractionation of an assemblage with a significant modal abundance of feldspar (+ quartz) over mica will result in a melt with higher Sn and W than the parental melt. Accessory minerals are also an important host of Nb, Ta, Sn and W within the source region, particularly Fe-Ti oxides (e.g. Stepanov and Hermann, 2013; Romer and Kroner, 2016). Tin partitioning during melting and fractionation is also partially influenced by the oxidation state of the melt. For example, in oxidising melts, Sn is stabilised as Sn^{4+}, which should result in partitioning into minerals such as biotite, hornblende and magnetite, and would therefore be more readily depleted during fractionation (Taylor and Wall, 1992). However, the Cornubian granites contain ilmenite, rather than magnetite, indicating their reduced nature and the linear increase in Sn versus $1/TiO_2$ (Fig. 4) implies Sn was relatively incompatible during fractionation.

The batch melting and Rayleigh fractionation equations (Eq. [A.1-A.2]), along with the average abundance of the rare metals from the Hu and Gao (2008) greywacke and the Gramscatho

greywacke source proxy were utilised. Additional data for metasedimentary rocks in the region from the study of Hall (1990) for Li, Nb and Sn were utilised to demonstrate the range of concentrations within metasedimentary rocks in the region. Major element and REE models indicated that 20% and 30% partial melting of a greywacke source would be sufficient to produce the element abundances shown in the G1-G2 and G3-G4 granites, respectively (Simons et al., 2016). Using these data 30% melting followed by 10% and 30% fractional crystallisation (G1-G2) and 40% fractional crystallisation (G3-G4) was modelled using the batch and Rayleigh fractionation models.

6.2. A fractional crystallisation model for distribution of rare metals in G1-G2 and G3-G4 granites

Prior to establishing the likely parental melt compositions, it is important to first consider the overprinting effects of fractional crystallisation. Fig. 4 indicates the strong influence of granite fractionation for several of the metals within the Cornubian Batholith. For G1-G2 granites, the modelled Li, Be, Nb, Ta, In, W and Bi abundances are consistent with fractionation of an assemblage comprising 20% biotite, 23% alkali feldspar, 50% plagioclase and minor garnet from the least evolved G1 granite to produce a more evolved G2 granite (Fig. 7, Supplementary Fig. 1a). There is likely minor quartz in the fractionating assemblage due to the high SiO_2 content of the melt, but quartz is excluded in these models due to lack of partitioning information. It is likely that the trace elements in this study have partition coefficients of significantly <1 for quartz due to low ppm concentrations (e.g. Drivenes et al., 2016) and a model without quartz therefore represents a minimum melt enrichment scenario for metal enrichment during fractionation. Across the batholith, modelled Sn abundances are slightly lower than observed concentrations, likely due to over-estimation of Sn compatibility. Modelled Nb and Sb abundances are slightly higher than observed concentrations, implying either an under-estimation of compatibility of these elements during fractionation or partitioning into a mineral not modelled, likely Fe-oxides for Nb. Gallium remains constant with fractionation (Fig. 7c). Up to 30% fractionation is required to account for the range of the G2 granites, with high Sn and W values in the sample from Hemerdon likely attributable to fluid-rock interactions (Supplementary Table 3).

A modified fractionating assemblage, comprising 25% biotite, 20% plagioclase, 50% alkali feldspar, minor cordierite and garnet is sufficient to model fractionation from G3 to more evolved G4 granites for Nb, Ta, In, Sn and Bi (Fig. 8, Supplementary Fig. 1b). Up to 40% fractionation is sufficient for the majority of observed G4 concentrations (Supplementary Table 4). Like G1-G2 granites, there is a discordance between observed and modelled Sb, with modelled Sb abundances higher than observed abundances, implying an under-estimation of the compatibility of Sb during differentiation. The Li, Ga and W concentrations within G4 granites do scatter slightly above modelled abundances compared to the models for G2 granites; the most evolved sample for modelling was chosen as one that does not display significant evidence for fluid fractionation, demonstrated by anomalies on trace element plots (Fig. 4). The scatters in Li, W and Bi are also likely attributable to element mobility associated with hydrothermal fluids, supported by modelling of Ba and Sr and variations in Rb/Sr (Simons et al., 2016).

6.3. Partial melting of a greywacke source

Fractional crystallisation modelling indicates the importance of this process for attaining high abundances of the trace metals in evolved granites, consistent with previous models for Sn, Nb and Ta (e.g. Lehmann, 1982; Stepanov and Hermann, 2013). Modelling of partial melting was undertaken to assess the source required to attain the metal abundances in the least evolved G1 and G3 granites. The samples representing the least fractionated partial melt are the least geochemically evolved; they are consistent with those identified in Simons et al., (2016). For the metals in this study, the least evolved sample has low Li, Be, Nb, Ta, Sn and W relative to other G1 samples. For the G1-G2 granites, there is a close match for modelled and observed Be, Ga, Nb, Ta, W and Bi abundances with 20% partial melting, utilising the Gramscatho Group greywacke samples as a proxy for a source (Fig. 9a). Indium and Sb have lower observed abundances, and Sn higher, within the least evolved G1 granite relative to modelled abundances, although the modelled In values are consistent with other G1 samples within the batholith. This may reflect under-estimated compatibility for In and Sb, and overestimated compatibility during melting for Sn. Minor Sn may also be contained within Fe-Ti oxides in the source.

Using a combined 20% partial melting and up to 30% fractional crystallisation model, the majority of the observed metal abundances within the G1-G2 granites can be accounted for, taking into account source heterogeneity (Fig. 7). Beryllium abundances scatter towards higher than modelled values using Gramscatho greywacke Be abundances; higher modelled abundances would be achieved if using the sedimentary source estimations of London and Evensen (2002) of 2-5 ppm (Fig. 7b). Lithium within the granites can be accounted for using the higher source abundance of Hall (1990) for shales within SW England, but not with the lower abundance (44 ppm) of Gramscatho greywacke, which may indicate a slightly enriched sedimentary source. Interbedded mudstone or mudstone-dominated packets would be expected in a greywacke-dominated succession. For Sb, the observed granite abundances fall well below modelled concentrations (Fig. 7), implying Sb is considerably more compatible than assumed given the available partitioning information.

For the least evolved G3 granite, up to 30% melting of a muscovite-depleted source produces a melt consistent with the observed Be, Ga, Nb, Ta, In, Sb, W and Bi abundances of G3 granites (Fig. 9b). Tin scatters towards higher observed abundances, likely a consequence of the role of F (see section 7.4), an overestimation of Sn partitioning during melting using the mineral/melt ratio from this study and/or higher temperature melting of the source and release of Sn from Sn-bearing Fe-Ti oxides. Lithium, which is significantly higher in the least evolved sample relative to the model (Fig. 9b) and Nb abundances across all G3 granites are largely accounted for by a higher source abundance due to source heterogeneity (Fig. 8a,d). For a combined partial melting, fractional crystallisation model, Ga, Sn and W show upward scatter in the granite abundances that is not accounted for by the models (Fig. 8), likely due to higher temperature melting incorporating Fe-Ti oxides or a slightly enriched source. Observed Be abundances also scatter upwards relative to models, but as with the G1-G2 granites, higher abundances can be accounted for by higher source values of 2-5 ppm. Sb shows lower abundances than expected from the models (Fig. 8h, Supplementary Table 4).

6.4. Evidence for mantle involvement in the melting and metal budgets

The granites are contemporaneous with lamprophyres dykes, sills and basalts (Dupuis et al., 2015). G3 and G4 granites also include mafic microgranular enclaves (MME) e.g. Stimac et al.

(1995). This is common with other granitic terrains, and raises the possibility of metal transfer between mantle- and crustally-derived magmas (e.g. Chappell, 1996; Štemprok and Seifert, 2010). The mantle contribution to the Cornubian Batholith appears to be confined to G3 granites and is minor (Darbyshire and Shepherd, 1994). Nevertheless, mantle He signatures are present in sulphide mineralisation associated with the earliest through to the latest granites and indicate persistent devolatisation of mantle-derived melts emplaced in the lower crust during batholith construction (Shail et al., 2003).

When the granite trace element data from this study are plotted with lamprophyre, basalt and MME data (Supplementary Table 1) there are no clear trends (Fig. 10). Granite data invariably scatter towards higher abundances, whilst MME, lamprophyre and basalt compositions lie generally towards lower abundance of the metals. Only Nb shows an increased abundance relative to the granites in this study, but there is no evidence for continuation of trends from mafic/ultramafic through MME to granites (Fig. 9b). Magma mixing would be expected to result in linear trends through all compositions, including MME, from mafic/ultramafic rocks towards the granites.

7. DISCUSSION

7.1. Concentration of metals by fractional crystallisation

Lithium, Be, Nb, Ta, Sn, In and W increase with granite fractionation in G1-G2 granites, and Li, Nb, Ta and Bi increase in the G3-G4 granites as expected due to their incompatible nature in a fractionating assemblage dominated by feldspars (e.g. for Sn, Lehmann, 1987) (Fig. 4). Gallium increases within G3-G4 granites but remains constant in G1-G2 granites. Ga is compatible in biotite, with $D^{Bt/Melt}$ of 3.1 (Ewart and Griffin, 1994), which is present in modelled fractionating assemblages for G1-G2 and G3-G4 granites. Providing biotite is in the fractionating assemblage, limited variation with fractionation is expected, consistent with the variations in Ga in the G1-G2 granites. The increase in Ga in the G3-G4 granites must therefore be attributed to higher source abundances, or increased degrees of partial melting of biotite. Indium shows similar behaviour to other lithophile metals such as

W, Nb and Ta, implying this metal is relatively incompatible during granite fractionation. Antimony shows no clear trend with fractionation. Upward scatter of observed trace elements relative to modelled abundances could reflect deviation from estimated source abundances, subsolidus or hydrothermal processes (Haapala, 1997) or devolatilisation of host rocks (Williamson et al., 2010). It is noted that whilst Sn and W are commonly associated, in SW England there appears to be a decoupling of these elements. Whilst both increase with fractionation, W shows a significantly stronger enrichment in the older G1-G2 granites whereas Sn increases more strongly in the younger G3-G4 granites (see Fig. 5). This is likely a consequence of the conditions of melting and availability of W and Sn over time, discussed further below.

Alternatively, the depletion of Li, In, Sn and W within evolved G4 granites, plotting away from the overall fractional trend may indicate losses during exsolution of magmatic-hydrothermal fluids. The globular tourmaline (G4b) subtype show lower abundances of Li, In, Sn, W and Bi relative to other G4 granites. Manning et al. (1996) suggested that G4b granites achieved water saturation, with loss of B from the melt, and therefore potentially Li, In, Sn, W and Bi. Depletion could also represent alteration of micas; Henderson et al. (1989) noted that this could result in the loss of Li along with Rb, Cs and F. G4b granites have snowball quartz textures with radial inclusions supporting fluid saturation (Müller and Seltmann, 1999). Equally, these granites may represent distinct pulses of melt from a fractionated magma chamber at depth (e.g. Merino et al., 2013). Both Nb and Ta increase strongly during fractionation crystallisation, particularly Ta which is less compatible than Nb in biotite (Stepanov and Hermann, 2013), with some suggestion that they are further concentrated by hydrothermal processes in the magmatic-hydrothermal transition, particularly in G2 granites (Ballouard et al., 2016), although Nb, Ta-rich rutile and columbite can be typical magmatic phases disseminated throughout a granite body. The scatter of Ta in G4 granites towards higher Nb/Ta at relatively constant Ta may represent variable melts not linked to the observed G3 granites; if Nb/Ta≤5 is a proxy for hydrothermal processes (Ballouard et al., 2016), these samples lie well within the magmatic field (Fig. 11).

The Hemerdon Granite is commonly an outlier on the models, with elevated abundances of Sn, W and Bi. This is not unexpected considering the extensive mineralisation in this area and the

difficulty in obtaining relatively unaltered samples. Thus these high abundances likely reflect fluid-rock interactions. Beryllium shows higher than expected concentrations in G2 granites for the G1-G2 fractionation model using a Gramscatho Group greywacke source abundance of 2.2 ppm. This might be attributable to source variation or incorporation into quartz which can occur during greisenisation (e.g. Williamson et al., 1997); greisen-style mineralisation is unequivocally spatially associated with G2 granites. Within the G3-G4 granites, the lower abundance of Be within the more evolved G4 granites appears to be controlled by strong partitioning of Be into cordierite. Beryllium has a partition coefficient of $D^{Crd/Melt}$ = 100 to >1000 and even a small modal abundance of cordierite in a fractionating assemblage will deplete any residual melt in Be (Evensen and London, 2003). Cordierite occurs in G3 granites, but not G4 granites, implying early crystallisation of this mineral in granites linked by fractionation (Simons et al., 2016), or crystallisation of cordierite in a deeper magma chamber prior to G4 melt extraction. Ultimately, in the Müller et al. (2006) study, metals such as Sn were shown to increase with granite fractionation in the G3-G4 granite series within the Land's End Granite; this is supported here and shown not only for Sn but additional metals such as Li, Ga, Nb, Ta, In, W and Bi across the batholith encompassing G1-G4 granites.

Highly evolved topaz (G5) granites in France and Germany have been interpreted as attaining their rare metal enrichment through fractionation from more voluminous, less evolved peraluminous melts (Raimbault et al., 1995; Breiter et al., 2005). However, fractionation trends shown by G1-G2 and G3-G4 granites do not translate into G5 granite compositions (Manning and Hill, 1990; Stone, 1992; Simons et al., 2016). A preferred model of biotite-dominated melting in the lower crust during granulite-facies metamorphism in the lower crust to liberate Li, Nb, Ta, Sn, W and F is preferred (e.g. Cuney and Barbey, 2014). There is a strong association between major NW-SE trending faults in the region and G5 granites. These faults may have aided extraction of low degrees of melt from the source region and transport to higher levels in the crust.

7.2. Partial melting of a metasedimentary source

Trace element modelling for the least evolved G1 and G3 granites shows that the abundances of a number of the metals in this study can be accounted for by up to 30% partial melting of a

sedimentary source, similar to a greywacke. Unlike in other regions within the Variscan belt, basement rocks are not exposed in SW England. South west England either represents Avalonian terrane or a similar, but separate, Gondwana-derived terrane (e.g. Shail and Leveridge, 2009; Nance et al., 2015). It is noted by Romer and Kroner (2014) that Avalonian sedimentary rock compositions show mixed enriched-"normal" signatures, with only small positive Sn anomalies. The Gramscatho greywackes, used as a peri-Gondwanan, starting compositional proxy, are compositionally similar to the average upper crustal abundances of Rudnick and Gao (2004) and greywackes of Hu and Gao (2008), with slight enrichment in Be, Ta and Bi and strong enrichment in Li. This indicates that a significantly enriched source may not be required in the Cornubian Batholith source rocks, in common with Avalonian geochemical signatures, but the partitioning of the metals into source minerals and temperature may be a key control.

Data from this study indicate that W partitions strongly into muscovite micas within the granites (Fig. 6). Muscovite micas are often the first minerals involved in incongruent melting reactions (Harris and Inger, 1992; Harris et al., 1995). If greywacke source micas are also enriched in W, any W that is not partitioned into residual minerals during melting will be released to the resultant melt. Metals such as Sn and Nb are hosted in muscovite (Fig. 6), but also in biotite and Fe-Ti oxides (e.g. Stepanov and Hermann, 2013); these are not melted until higher temperatures are attained. Higher temperature melting will potentially release increased abundances of metal hosted in biotite and Fe-Ti oxides to the melt, reducing the need for extreme fractionation, but also lowering the requirement for low degrees of partial melting of an enriched source.

The low Nb within the least evolved G1 granite, relative to modelled Nb abundances of melting a Gramscatho greywacke source (Fig. 9a), is likely linked to partitioning of Nb into residual minerals during melting or retention of Nb in Ti-oxides not accessible at conditions of minimum melting. This study indicates that biotite can both host Nb and Ta, confirming previous studies (Bea et al., 1994; Stepanov et al., 2014). The Nb partition coefficients will vary, dependant on the Ti-abundance within the source biotite and degree of equilibrium between source Fe-Ti oxides and melt (Marschall et al., 2013). During melting of metasedimentary sources, Nb can partition into residual biotite and Fe-Ti oxides; the former may be consumed during higher degrees of partial melting or

melting at higher temperatures (Spear et al., 1999; Stepanov and Hermann, 2013; Stepanov et al., 2014). The G3 granites resulted from higher temperature melting that was dominated by biotite breakdown, but with consumption of Fe-Ti oxides also likely (Chappell and Hine, 2006; Simons et al., 2016), and hence are characterised by high Nb in the parental melt (see also discussion surrounding mica melting in Romer and Kroner, 2016). G3 granites were emplaced during a period of tectonic extension in SW England and higher melting temperatures are aided by continued emplacement of mantle-derived melts in the lower crust.

The combined melting and fractional crystallisation models show a good match between modelled and observed abundances for the majority of the elements. In both the G1-G2 and G3-G4 granites, there are discrepancies between modelled and observed abundances, when utilising the Gramscatho greywacke as a proxy for source abundance. Whilst this can largely be accounted for using the greywacke values of Hu and Gao (2008) to account for source heterogeneity, Sn and Sb still show a discordance between modelled and observed abundances. The Sn discrepancy could result from an over estimation of the compatibility of Sn in mica or melting of a slightly enriched source, as suggested by Romer and Kroner (2016) for the Cornubian granites. The mineral/melt ratio utilised from the mineral chemistry data in this study for mica (up to 2.32) is likely an over estimate of the true partition coefficient. As a melt evolves, the Sn partition coefficient is likely to reduce for mica, as B, OH and F increase, helping to increase diffusion and extend enrichment of metals such as Sn within the residual melt (Pollard et al., 1987). Assuming complete incompatibility of Sn, 30% melting and up to 50% fractionation was shown by Williamson *et al*. (2010) to account for the range of Sn observed in the Cornubian granites. This study demonstrates that Sn is compatible in biotite and muscovite and in all likelihood the true partition coefficient must lie between 0 (Williamson *et* al., 2010) and 2.32 (this study). Quartz was also not modelled in the fractionating assemblage in this study to give a minimum melt enrichment scenario for metal enrichment during fractionation. Given the compatibility of Sn in biotite and Fe-Ti oxides, it could also be assumed that not all Sn will be released to a melt during partial melting and may be retained in the source during early muscovite-dominated melting, only being released to a melt at higher temperatures of partial melting.

The partitioning of Sb is either under-estimated in the main silicate minerals or alternatively, the lack of correlation on the plot of $1/TiO_2$ vs. Sb might indicate that Sb is not controlled by granite crystallisation processes. There are few previous studies of Sb partitioning, but one, of a basanitic melt, indicates that Sb has a strong preference for garnet, not micas (Adam and Green, 2006). It is not clear into which mineral(s) Sb partitions. However, the failure of the model, coupled with lack of evidence of a granite control leads to the conclusion that Sb distribution in SW England is not dominantly controlled by granite-related magmatic processes. Much of the documented Sb mineralisation in the region occurs in Carboniferous pre-granite shear zone veins and is not associated with granite-related mineralisation styles (e.g. Clayton and Spiro, 2000).

7.3. The role of the mantle

A contribution to the metal budget from a mantle source is not required or supported by the observed variations, converse to the theory of Seifert (2008) for the origins of Sn and W in the granites of the Erzgebirge, Germany. Interpretation of enclave geochemistry is problematic due to chemical exchange of element between the host granite melt and enclave, obscuring the original mafic composition of the enclave (e.g. Stimac et al., 1995). Mixing models for individual elements may not be consistent between different samples due to variable advection and/or diffusion processes (Orsini et al., 1991; Perugini et al., 2008). Whilst the mixing behaviour of the elements in this study remains largely unknown, it is noted by Tindle (1991) there will be more chemical exchange of large ion lithophile elements (LILE) due to their large ionic radius to charge ratio and compatibility in both granite and enclave minerals. Lithium also behaves as a LILE due to its radius to charge ratio, despite a small ionic radius. High field strength elements (HFSE) such as Nb, Ta and W have high charges and are generally less mobile as it is difficult to maintain charge balance. It is therefore thought that the enrichment of the metals (Li, Sn, W) in the enclaves relative to the lamprophyres and basalts represents chemical exchange of these elements between the granitic melt and original melt; this is also noted for other incompatible elements such as Th and U by Stimac et al. (1995). Given the amount of chemical exchange between enclaves and their granite hosts it may be impossible to

determine the extent of mixing; for this an enclave that has undergone no chemical exchange would be needed.

7.4. The role of fluorine and phosphorus

Although F wasn't analysed as part of this study, F appears to be a key control on the distribution of Nb, Ta, Sn, W and to a lesser extent In, within the Cornubian batholith. Using previous data, there is a moderate increase in F in the G1-G2 granites from approximately 0.2% F (Charoy, 1986; Chappell and Hine, 2006) in G1a granites of the Carnmenellis pluton to approximately 0.4% F in the smaller G2 granite stocks such as Cligga and St. Michael's Mount (Hall, 1971; Moore and Jackson, 1977). For the G3-G4 series, F increases from approximately 0.2% in the biotite granites to approximately 0.7% F in the tourmaline granites of the St. Austell Granite (Hill and Manning, 1987). G5 granites contain F in excess of 1 wt.% (Manning and Hill, 1990). Increased F is common in fractionated peraluminous melts and along with other fluxing elements such as B and P lowers the temperature of the melt (Černý et al., 2005). High F promotes the retention of Nb, Ta and W within a low temperature melt, with these metals partitioning in favour of a melt during melt evolution. As the F content of a melt decreases during crystallisation of F-bearing minerals, Nb, Ta and, to a lesser extent, W, will increasingly partition into silicates (e.g. micas) and oxides (e.g. rutile, columbite, wolframite) if the melt is saturated with respect to these minerals (Manning and Henderson, 1984; Keppler, 1993; Linnen, 1998). This is observed in the Cornubian Batholith as the granites with the highest F contents (G4 and G5) show the highest Nb and Ta (Fig. 4). Within the trioctahedral micas, Nb and Ta have a negative correlation with F, supporting their incorporation into accessory minerals rather than major silicates (Supplementary Fig. 3). The G4 granites contain columbite-tantalite and Nb-rich rutile (Scott et al., 1998) and data from this study indicate Nb and Ta are controlled by accessory minerals (Fig. 6e-f). Metal distribution also implies that Sn, W and minor In are controlled by high F; the G4 and G5 granites with high F, have accessory minerals hosting Sn, W and In (Fig. 6f).

The topaz granites are an "anomaly" in SW England and do not exhibit the geochemical characteristics of the G1-G2 or G3-G4 granites. Fractionation of a G1 or G3 granite melt to produce a

topaz (G5) granite is problematic, as linear relationships on bivariate major and trace element plots and field relations cannot be resolved (e.g. Manning and Hill, 1990; Stone, 1992; Simons et al., 2016). Conventional fractionation models, as applied to the G1-G2 and G3-G4 granites, do not therefore apply to the G5 granites. A model of flux-induced melting of lower crustal source containing biotite during granulite facies metamorphism is preferred (Stone, 1992; Cuney and Barbey, 2014; Simons et al., 2016). Melting of biotite would likely liberate Li, Nb, Ta, Sn and F, with minor In and W into a melt (Fig. 6). Extension in SW England at the time of granite emplacement supports the influx of mantle-derived melts into the lower crust and subsequent high temperature, low-pressure conditions. High F in a source, would also be beneficial for transport of HFSE (Sn, Nb, Ta and W). Fluorine contents are higher in the topaz granites compared to the all other granite types (e.g. Stone, 1992) and the distribution of Nb, Ta, In, Sn and W is controlled by accessory minerals including Nb-bearing rutile, cassiterite and columbite. Granites that evolve towards or have high F contents can be characterised by the occurrence of disseminated magmatic mineralisation, depending on depth of intrusion, with limited partitioning of metals such as Sn and W into fluids exsolved from the melt (e.g. Pollard et al., 1987). In SW England, the G5 granites have F-bearing minerals such as F-rich micas, F-rich topaz and primary fluorite, implying early retention of F in the melt, rather than F-rich fluid exsolution. Accessory cassiterite is reported from G5 granites (Stone et al., 1988).

Phosphorus, like F, increases with fractionation of a peraluminous melt, and is highest in the evolved granites in SW England that have the lowest Ca. High-P with low Ca, termed the "Pedrobernardo trend" by Bea et al (1992), causes P to behave as an incompatible element, concentrating within residual fluids, as apatite crystallisation is limited by the lack of Ca. Unusual phosphates, such as amblygonite and triplite, found within G5 granites, are also able to crystallise (Stone and George, 1978, 1983). There is a positive correlation between P_2O_5 and Rb, commonly concentrated in residual melts, and a negative correlation between P_2O_5 and compatible elements such as Sr and Ba within the Cornubian Batholith (Simons et al., 2016). Applying this to the rare metals, there is a positive correlation, with some scatter, for Be, Nb, Ta, In, Sn, Ta, W and Bi for G1-G2 granites, with no overall trend for Li, Ga and Sb. For G3-G4 granites, Li, Ga, Nb, Ta, In, Sn, Ta and Bi show a positive correlation, Be a negative correlation, and there is no overall trend for Sb, W and

Bi (examples in Fig. 12). Scatter towards lower abundances in G4 granites is confined to the globular quartz variant (G4b); these plot towards higher P_2O_5 which supports fluid alteration of these samples, as discussed above. The combined effects of F and P, along with Li, appear to favour retention of Nb, Ta, In, Sn, W and to a lesser extent Be, Ga and Bi within the melt and hence increase the potential, depending on late magmatic evolution, for subsequent partitioning into exsolving magmatic-hydrothermal fluids.

7.5. Biotite micas as indicators of magmatic evolution

As previously demonstrated by Stone et al. (1988), trioctahedral micas are particularly effective at recording evolving melt compositions within the batholith. Using Mg-Li (apfu) as a differentiation index, the trace elements form clear trends (Tischendorf et al., 1997; Tischendorf et al., 2001). Tungsten increases with mica evolution from G1 to G5 granites, with decreasing Mg and increasing Li (Fig. 13a). The strong enrichment of W with increasing Li can be attributed to the overall incompatible nature of W within felsic melts, consistent with whole rock trends (Fig. 4i). Niobium decreases within the trioctahedral micas (Fig. 13b), showing similar trend to F (Supplementary Fig. 2), and confirming partitioning into trace minerals. Tin, In and Ga increase from Mg siderophyllite to zinnwaldite, with a marked decrease in lepidolite (Fig. 13c-d). This trend is noted for Sn in trioctahedral micas by Tischendorf et al. (2001). It could imply crystallisation of lepidolite after Ga, Sn and In have already been exsolved from the magma within magmatic-hydrothermal fluids, which could potentially also remove Li and F, or crystallisation of mica after crystallisation of disseminated magmatic cassiterite. Granite evolution is tracked by major mineral chemistry in several other granite terrains. Within the peraluminous Variscan granites of Portugal and Germany, variations in mineral chemistry also reflect evolution of the host granite and minerals such as micas are useful indicators of the melt composition at the time of crystallisation (Tischendorf et al., 2001). Similar to mineral chemistry in SW England, evolved granites from Germany and Portugal contain evolved micas such as zinnwaldite (e.g. Förster et al. 1999; Neiva et al. 2011).

7.6. Implications for magmatic-hydrothermal mineralisation

Radiometric dating of granites and associated mineralisation indicates that each pluton has its own discrete episodes of magmatism and mineralisation and there is not a region-wide fluid source for the mineralisation (e.g. Chen et al., 1993; Chesley et al., 1993; Clarke et al., 1993). Given the composite nature of the batholith, multistage emplacement of G1-G5 granites beneath the current exposure level is a distinct possibility, with multiple stages of fluid exsolution and fluid transport to higher levels within the crust via deep crustal faults. However, the in situ differentiation of the granites, with fractionation of Sn-W and associated metals is demonstrated at the current exposure level. There are contrasts in the rare metal magmatic-hydrothermal mineralisation between the two major episodes of magmatism represented by the G1-G2 and G3-G4 granites, and also the volumetrically minor (at the current exposure levels) G5 episode. These granite suites have potentially exsolved rare metals in differing relative proportions due to the variations source melting conditions and subsequent fractionation.

Lithium is fairly ubiquitous across the study area, occurring within trioctahedral and dioctahedral micas and tourmaline and increasing with fractionation. The strongest enrichment of Li is within the G5 granites and topaz aplites. The G5b pegmatites, similar to those associated with the Tregonning Granite, may represent a potential source of Li-rich minerals, but these pegmatites are volumetrically minor, similar to the Li-Cs-Ta-type pegmatites described elsewhere, for example in the Moldanubian Zone of the Bohemian Massif, Czech Republic (e.g. Breiter, 2014). Lithium enrichment in Li-Fe micas, particularly prevalent in the G4 and G5 granites could represent a source of Li.

Beryllium has divergent behaviour between the G1-G2 and G3-G4 granites. There is a strong increase in Be within the G1-G2 granites, implying that hydrothermal fluids exsolving from the more evolved G2 granites may be enriched in Be. Any pegmatite associated with this granite series would be expected to carry Be minerals, consistent with descriptions of beryl and bertrandite within the Trolvis Quarry pegmatite of the Carnmenellis G1 granite (Hosking, 1954). Conversely, Be is depleted in the most evolved G4 granites because of its removal by cordierite fractionation.

In both the G1-G2 and G3-G4 granites, Sn and W increase with fractionation. However, there are key differences between these two suites that result in a decoupling of Sn and W mineralisation between them. Tungsten enrichment in granites and their associated magmatic-hydrothermal

mineralisation is more strongly associated with the older G1-G2 granites. In contrast, Sn is fairly ubiquitous across both suites but shows a consistent increase with fractionation in younger G3-G4 granites. This is likely to be controlled, in part, by contrasting source melting temperatures between the two suites. For early granites, the melting temperature was lower, which resulted in muscovite-dominated and minor biotite melting. If W was dominantly hosted within source muscovite, and Sn within source biotite and Fe-Ti oxides, W will be melted out of the source first. As extension in SW England continued, further underplating and/or lower crustal sill emplacement of mantle-derived melts caused increasing temperatures, biotite and Fe-Ti oxides become involved in melting reactions and release additional Sn to the G3-G4 melts.

In the evolved G2 granites, Sn and W are hosted within muscovite micas. Muscovite is both primary and late-stage magmatic/subsolidus in G2 granites. Both primary (muscovite) and late-stage (Li-Fe muscovite) contain comparable Sn, with slightly higher W in the latter (Table 3). This implies that Sn and W in muscovite may partition into fluids that exsolve from cooling muscovite (G2) granites as late-stage muscovite should represent the magmatic-hydrothermal transition. It has been suggested by Neiva (1987) that biotite breakdown in already crystallised granite will liberate metals such as Sn and W, making them available for mineralisation. Although such a model is not thought to be a dominant source for Sn and W in SW England mineralisation, these elements will be redistributed during biotite alteration to chlorite (e.g. Alderton et al., 1980). G2 granites are spatially associated with Sn-W/W-Sn greisen deposits in the region. If muscovite is also the dominant host for W within the source, these metals will partition into the earliest formed crustal melts and hence will be associated with the older G1-G2 granites.

Within the G3-G4 granite series, tourmaline is the dominant late-stage magmatic mineral, rather than muscovite, although accessory (secondary) muscovite is still present. Both Sn and W are dominantly hosted within Li-rich micas in G4 granites and could be readily redistributed by hydrothermal fluids. Finally, the G3-G4 system is associated with strong increases in Li, F. Boron also increases, indicated by the increased modal abundance of tourmaline and presence of late-stage orbicules (e.g. Drivenes et al., 2015), indicating the system is evolving towards possible miscibility between boron-rich melts and/or fluids This implies, that unlike Sn, W is not preferentially enriched

in boron-rich melts or fluids that presumably remain towards the later stages of crystallisation (Figure 5 for Sn-W distribution). This is in part supported by experimental work demonstrating that in the presence of a B-rich fluid, W is preferentially retained in melts rather than partitioning into hydrothermal fluids exsolving from cooling granitic bodies, whereas Sn is commonly associated with quartz-tourmaline lodes in the region (Manning and Henderson, 1984).

Indium increases with fractionation in the G1-G2 and G3-G4 granite series. Like Sn and W, In is hosted within muscovite in the G2 granites, implying that In is incompatible in this fractionation trend and may be available for partitioning into hydrothermal fluids that exsolve from these granites. Within the G3-G4 granites, In also increases, like Sn and W, but is partitioned into Li-rich micas and tourmaline. However, unlike Sn and W, In mineralisation is preferentially hosted by sulphides rather than oxides (Andersen et al., 2016) implying a mechanism that requires the presence of sulphur for precipitation of In-bearing minerals or substitution into other sulphides.

Within evolved G2 granites, Nb and Ta are hosted within muscovite, biotite group minerals (if present), Fe-Ti oxides and columbite-tantalite group minerals. As muscovite is late-stage and biotite group minerals will readily undergo breakdown during hydrothermal alteration, this may provide a mechanism for incorporating Nb and Ta into magmatic-hydrothermal fluids associated with evolved G2 granites, if Nb and Ta have not already been sequestered to form disseminated Nb-Ta-rutile and / or columbite disseminated throughout the granite. Both Nb and Ta increase with fractionation in the G3-G4 granites. However, in the G4 and G5 granites, the distribution of Nb and Ta is dominantly controlled by accessory minerals such as rutile and columbite, disseminated throughout the granites (Scott et al., 1998), implying limited potential for their partitioning into magmatic-hydrothermal fluids.

Gallium is distributed fairly evenly between the major minerals in all granite types and exhibits limited correlation with fractionation. Feldspars and micas readily undergo hydrothermal alteration and this may control Ga content in magmatic-hydrothermal fluids. Gallium has higher abundances in G4 granites and therefore may be preferentially associated with these granites, but there are no data on the distribution of Ga in SW England granite-related mineralisation. Antimony is

not enriched by fractionation in the granites and Sb mineralisation in the region is therefore unlikely to be granite derived.

Differentiation in the G1-2 granite series increases all metals apart from Ga and Sb. The G2 granites are strongly correlated with regional sheeted vein greisen W-Sn mineralisation across the region. Our study also supports the suggestion of Müller et al. (2006) that the G4 granites within the northern part of the Land's End Granite are the immediate magmatic precursors to tourmaline-dominated magmatic-hydrothermal mineralisation in the region. The G5 granites evolve towards very low-grade disseminated Sn-Ta-Nb-(W) magmatic mineralisation; this has not been exploited. The role of G5 granites in controlling W-Sn magmatic-hydrothermal mineralisation is unclear; it has been suggested that they are surrounded by tourmalinised alteration haloes that relate to volatile exsolution (e.g. Manning and Hill, 1990). However, it is clear that Sn-Ta-Nb-(W) is retained more effectively in the magmatic system than for the G1-G2 and G3-G4 granites. The G5 granites are worked for kaolin in the St. Austell and Dartmoor granites.

7.7. Global analogues

Mineralised granites can develop from either unenriched or enriched sources as most rare and base metals of interest tend to be incompatible and so can be enriched during melting and granite fractionation (e.g. Lehmann, 1982; 1987). Fractional crystallisation is enhanced by the presence of fluxing elements (e.g. B, P, F), high K, shallow crustal settings and high temperatures (e.g. Černý et al., 2005), all of which are characteristics of the granites of SW England. Other localities with peraluminous granites and rare metal mineralisation such as the Variscan granites of the Erzegebirge, Germany and the Jingnan granites, Dahutang area, China, have also formed from both enriched and unenriched sources, with concentration of rare metals (Li, Sn, W, Ta, Nb, Bi) enhanced by the presence of fluxing elements, temperature of melting and high levels of crustal emplacement (e.g. Breiter, 2012; Huang and Jiang, 2014). The Variscan Carrazeda de Ansiães granites in Portugal formed from heterogeneous metapelites, and like the Cornubian Batholith from a source relatively unenriched in Sn and W; fractional crystallisation in the presence of F and B was sufficient to increase metals in the granites prior to exsolution of Sn-bearing hydrothermal fluids (Teixeira et al., 2012). Tin

and W in two-mica and muscovite granites in Portugal differentially partition into muscovite (Neiva et al., 2002) and are therefore similar to the Cornubian Batholith. Partial melting of variably enriched metasedimentary rocks followed by fractional crystallisation processes have previously been invoked as a method for enriching metals such as Sn and W (and fluxing elements) within other European Variscan granites (e.g. Romer and Kroner, 2016) (e.g. Kováříková et al., 2007; Breiter, 2012) and China (e.g. Huang and Jiang, 2014). There is limited information available about In within peraluminous granites. However, within the mineralisation associated with the highly evolved A-type granites of the Wiborg Batholith, Finland, there is significant In incorporated into sulphides (Haapala and Lukkari, 2005; Cook et al., 2011b). There may be a similar increase of In with granite fractionation associated with this locality, as reported for melt inclusions for the area (Lukkari et al., 2009).

The topaz (G5) granites are most similar to descriptions of RMG (Černý et al., 2005). With regards to the metals in this study, peraluminous RMG are characterised by the presence of extreme enrichment of Li, Be, Nb, Ta, Sn and W and disseminated magmatic mineralisation, promoted by high-F, Li and/or P. Variscan RMG with associated disseminated magmatic mineralisation include the Beauvoir Granite, Massif Central (Marignac and Cuney, 1999) and Podlesí Stock, Czech Republic (Breiter et al., 1997). The former is interpreted as forming from a rare metal-enriched fluid derived from the breakdown of biotite during granulite facies metamorphism (Cuney and Barbey, 2014), and the latter through extreme fractionation (Breiter et al., 1997). The Yichun RMG granite complex of SE China comprises disseminated columbite and cassiterite, and formed through multiple stages of fractional crystallisation (Belkasmi et al., 2000).

8. Conclusions

1. The Early Permian post-Variscan Cornubian Batholith is composite, constructed over 20 Ma. An older stage of magmatism, generated during muscovite-dominated and minor biotite melting of a metagreywacke source formed two mica (G1) granites, with fractionation to form muscovite (G2) granites. Continued extension and underplating of mantle-derived melts, induced higher temperature, biotite-dominated melting, leading to a second major stage of magmatism,

producing biotite (G3) granites and fractionated tourmaline (G4) granites. Minor topaz (G5) granites form from flux-induced melting of biotite in the lower crust.

2. Lithium, Be, Nb, Ta, Sn, W and Bi are enriched in the granites of the Cornubian Batholith relative to average crustal abundances. Topaz (G5) granites have the highest Li (mean 1363 ppm), Ga (38 ppm), Nb (52 ppm), Ta (15 ppm), Sn (21 ppm) and W (24 ppm) relative to the remaining G1-G4 granites. Beryllium is most strongly enriched in muscovite (G2) granites (mean 12 ppm) and Bi in tourmaline (G4) granites (mean 0.94 ppm). Indium has a consistent abundance in the granites relative to crustal abundances, with G4 granites having the highest modal abundance (mean 90 ppb). Sb has lower abundances in the granites compared to average crustal abundances.
3. Fractionation, dominated by biotite and feldspars, increases Be, Nb, Ta, In, Sn, W and Bi in the G1-G2 granites. Gallium remains constant and Sb shows no overall trend. Within the G3-G4 granites, Li, Ga, Nb and Ta increase strongly with fractionation. Beryllium decreases, due to cordierite fractionation, and Sb and Bi show no overall trend. Several In, Sn and Bi values scatter towards lower abundances in the G3-G4 granites due to fluid involvement, particularly in the globular quartz facies.
4. Trace element modelling indicates that 20% partial melting of a greywacke source and up to 30% fractionation is sufficient to account for the range of observed abundances of the metals in G1-G2 granites. In G3-G4 granites, 30% partial melting and up to 40% fractionation is sufficient for the majority of elements. Observed Nb and Ta abundances scatter upwards relative to modelled values, facilitated by high F. Observed Sb lies far below modelled concentrations. There is no evidence for a mantle source using the constraints provided here.
5. G5 granites form from fluid fluxed melting of a biotite-rich source. This source would be enriched in F, Li, Nb, Ta and Sn hosted within source biotite, producing a melt enriched in these elements, consistent with the G5 topaz granites in SW England and RMG such as the Beauvoir Granite, Massif Central, France.
6. Lithium is dominantly hosted by trioctahedral micas across all granite types. Gallium is distributed fairly evenly between all major silicates. Niobium and Ta partition into muscovite in

G1-G2 granites, trioctahedral micas in G3 granites and accessory minerals in G4 and G5 granites, although Fe-Ti oxides are an important host in all granite types and columbite-tantalite host Nb and Ta in G5 granites. Indium, Sn and W follow Nb and Ta, with the exception of G4 granites, in which they are incorporated into trioctahedral micas.

7. There is a strong spatial associated between W-Sn greisen deposits and G2 granites, e.g. Hemerdon, Cligga and St. Michael's Mount. The metals partition dominantly into muscovite, with limited disseminated magmatic mineralisation. G4 granites are likely precursors to tourmaline-dominated magmatic-hydrothermal mineralisation and represent sources of Sn, for example in the mineralisation north of the Land's End Granite and tourmaline-dominated systems around the St. Austell Granite. Beryllium is not associated with G4 granites. Phosphorus and F cause the retention of Nb, Ta, Sn, W and to a lesser extent, In, in the melt. In G4 and G5 granites with high P (>0.4 wt. %) and F (>1 wt.%), this promotes disseminated magmatic mineralisation. High F promotes disseminated magmatic mineralisation through lowering melt temperature resulting in retention of HFSE in the melt. On crystallisation of an F-bearing mineral, minerals such as columbite precipitate, providing melt saturation is achieved (e.g. Linnen, 1998).
8. There is a decoupling of W and Sn behaviour in SW England. Whilst both increase with fractionation, W shows a significantly stronger enrichment in the older G1-G2 granites whereas Sn increases more strongly in the younger G3-G4 granites. This is likely a consequence of increasing temperatures in the lower crustal source region that progress from lower temperature muscovite-biotite (W ≈ Sn) melting to higher temperature biotite-dominated melting (Sn > W).
9. G1-G2 granites are similar to two-mica and muscovite-bearing granites of Portugal associated with W mineralisation, formed through partial melting of unenriched greywacke sources, with metal enrichment via fractional crystallisation. Analogues of G3-G4 granites include granites within the Variscan zone in Germany and Spain, which are also fractionated sedimentary-sourced melts.

Acknowledgments

This study was supported by the European Regional Development Fund and European Social Fund as part of the convergence funding for Cornwall and the Isles of Scilly supporting a PhD for BS (Combined Universities in Cornwall project number11200NCO5) and the European Union (Horizon 2020 project 641650 FAME). The LA-ICP-MS work was supported by a grant from the Natural Environment Research Council (NERC, NE/L001896/1). The Cornwall Heritage Trust are thanked for providing additional funds for analysis. The Natural History Museum, London, UK are thanked for loan of samples from collection BM.2004,P14, specimen numbers 1, 7, 8, 10, 21, 23, 24, 30 and 31 and thin sections P11849, P11851, P11864, P12400 and P12399. Samples GG6, GG15, GG28, and GG44 from the study of Darbyshire and Shepherd (1994) came from Peter Floyd, University of Keele. Steve Pendray, Sharon Uren and Joe Pickles assisted with the sample preparation and analysis at Camborne School of Mines. Sam Hammond assisted with LA-ICP-MS analysis at the Open University. De Lank, Carnsew and Castle-an-Dinas quarries, Richard Scrivener, Nick LeBoutillier and Ben Thompson (Imerys) are thanked for help with sampling. Karel Breiter and one anonymous reviewer are thanked for their generous and constructive comments which have helped to improve the manuscript.

Appendices

Eqs. A.1-2 Trace element modelling equations and partition coefficients

After Shaw (1970):

[Eq. A.1] Batch melting: $C_L / C_O = 1 / [D + F(1-D)]$

[Eq. A.2] Raleigh fractionation: $C_L / C_O = F^{(D-1)}$

where:

C_L =Weight concentration of a trace element in the melt

C_O =Weight concentration of a trace element in the source

D =Bulk distribution coefficient for residual solids (batch melting) or the fractionating assemblage (Raleigh fractionation)

F = Weight fraction of melt produced (batch melting) or the fraction of melt remaining (Raleigh fractionation)

Table A.1 Partition coefficients used for partial melting and fractionation crystallisation modelling.

	Qtz*	**Kfs**	**Pl**	**Bt**	**Msc**	**Grt**	**Sil**	**Crd**
Li	0	0	0	1.65[1]	0.80[1]	0	0	0.44[2]
Be	0	0.26[2]	0.10[2]	0.39[2]	1.35[2]	0	0	30.69[2]
Ga	0	0.20[3]	0.59[3]	3.10[3]	5.04*	0	0	0
Nb	0	0.04[3]	0.07[3]	1.96[5]	0.15[5]	0	0	0.01[1]
In	0	0*	0*	1.87*	5.21*	10.3[4]	0	0
Sn	0	0.05*	0.60*	2.32*	4.14*	0.86[4]	0	0
Sb	0	0	0	0.0013[4]	0	10[4]	0	0
Ta	0	0.025[6]	0.063[7]	0.16-0.91[5]	0.06-0.45[5]	0.0017[4]	0	0
W	0	0*	0*	0.4*	10.71*	0.0008[4]	0	0
Bi	0	0	0	0	0	0	0	0
	Melting abundances							
G1	0.45	0.02	0.35	0.12	0.02	0.03	0.01	0
G3	0.45	0	0.40	0.12	0	0.01	0.01	0.01
	Fractionating assemblage							
G1-G2	0**	0.23	0.50	0.22	0	0.046	0	0
G3-G4	0**	0.24	0.50	0.25	0	0	0	0.01

All zeros, unless otherwise stated, are estimated as 0, in part due to high charge and large ionic radii, following the methods of Williamson *et al*, 2010. (1) Icenhower and London, 1995; (2) Evensen and London, 2002; (3) Ewart and Griffin, 1994; (4) Adam and Green, 2006; (5) Stepanov and Hermann, 2013; (6) Mahood and Hidreth, 1983;(7) Streck and Grunder, 1997. *Estimated mineral/melt ratio from this study. Calculated by dividing mineral (LA-ICP-MS) by whole rock abundance (ICP-MS). Melting abundances and fractionating assemblages from Simons et al. (2016). **Set at 0 for this study due to lack of partition coefficients for quartz and assumed incompatibility; there is likely to be a minor amount of quartz in a fractionating assemblage.

Appendix references

Adam, J., Green, T., 2006. Trace element partitioning between mica- and amphibole-bearing garnet lherzolite and hydrous basanitic melt 1: Experimental results and the investigation of controls on partitioning behaviour. Contributions to Mineralogy and Petrology 152, 1-17.

Evensen, J.M., London, D., 2002. Experimental silicate mineral/melt partition coefficients for beryllium and the crustal Be cycle from migmatite to pegmatite. Geochimica et Cosmochimica Acta 66, 2239-2265.

Ewart, A., Griffin, W.L., 1994. Application of proton-microprobe data to trace-element partitioning in volcanic rocks. Chemical Geology 117, 251-284.

Icenhower, J., London, D., 1995. An experimental study of element partitioning among biotite, muscovite, and coexisting peraluminous silicic melt at 200 MPa (H_2O). American Mineralogist 80, 1229-1251.

Stepanov, A.S., Hermann, J. 2013. Fractionation of Nb and Ta by biotite and phengite: Implications for the "missing Nb paradox". Geology 41, 303-306.

Streck, M.J., Grunder, A.L., 1997. Compositional gradients and gaps in high-silica rhyolites of the Rattlesnake Tuff, Oregon. Journal of Petrology 38, 133-163.

Williamson B.J., Müller A., Shail R.K., 2010. Source and partitioning of B and Sn in the Cornubian Batholith of southwest England Ore Geology Reviews 38:1-8

Figures

Fig. 1. Geological map of SW England showing the principal mineralogical and textural variations in the Cornubian Batholith and subdivision of G1-G5 granites. Compiled from Ghosh (1927), Exley and Stone (1982), Dangerfield and Hawkes (1981), Manning et al. (1996), Selwood et al. (1998), Müller et al. (2006) and British Geological Survey data (Geological Map Data © NERC 2016). Reproduced after Simons et al. (2016).

Fig. 2. Field photographs of Cornubian Batholith granites. **a** – Typical G1a granite with orthoclase phenocrysts (<25 mm) from the Carnmenellis Granite. **b** – Enclave of G1c granite within G1a granite, St. Agnes, Isles of Scilly Granite. **c** – Cligga G2 Granite with sheeted W greisen veins. **d** – Coarse-grained porphyritic G3a granite with abundant orthoclase phenocrysts (>25 mm) from the Dartmoor Granite. **e** – Globular quartz G4b granite from Carn Dean Quarry, Land's End Granite. **f** – Pegmatitic pocket dominantly comprising tourmaline, orthoclase and quartz within G3a granite, Land's End Granite. **g –** Typical topaz (G5) granite texture, equigranular with abundant Li mica, Tregonning Granite.

Fig. 3. Multi-element plot showing average metal abundances normalised to the upper continental crustal (UCC) values of Rudnick and Gao (2004). Regionally, there is a strong enrichment in Li in all granites and G2 and G5 granites show strong enrichment in W. Gallium, In and Sb plot towards expected UCC abundances. Beryllium, Nb, Ta, Sn and Bi are slightly enriched in the least evolved G1 and G3 granites, typically increasing for G2, G4 and G5 granites. Average values for the peri-Gondwanan Devonian Gramscatho Basin (GB) plot around average UCC abundances.

Fig. 4. Trace element variation diagrams using $1/TiO_2$ as a differentiation index for **a –** Li, showing a positive trend for both G1-G2 and G3-G4 granites; G5 granites plot towards extreme values. The circled G4 granites show low Li attributable to alteration. **b** – Converse trends for Be, increasing with fractionation in G1-G2 and decreasing in G3-G4. **c –** Positive curvilinear trend for Ga for G3-G4 granites and no trend for G1-G2 granites (constant abundance with fractionation). **d** – Curvilinear positive trends for Nb in G1-G2 and G3-G4, with stronger enrichment in the latter. G5 granites plot towards extreme Nb values, with a distinctive gap between evolved G2 / G4 granites and G5. **e** – Curvilinear positive trends for Ta, with stronger correlations for G1-G2 granites with fractionation. Scatter in the G3-G4 granites is likely an effect caused by evolution towards high-F melts and changes in partitioning behaviour of Ta into accessory minerals (see discussion). **f** – Trends for G1-G2 and G3-G4 granites show increasing In with fractionation. G5 granites plot towards low In. The circled G4 granites show low In attributable to alteration. **g** – G1-G2 granites have a curvilinear positive Sn correlation with granite fractionation. G3-G4 granites broadly increase but there is no comprehensive correlation. Low values of Sn are likely attributable to alteration. G5 granites plot towards high Sn. **h** – There is no conclusive trend observed for any granites with Sb. **I** – W increases strongly within G1-G2 granites but shows no conclusive correlation with fractionation in the G3-G4 granites. G5 granites plot towards high W abundances, with a distinctive gap between the most evolved G2 and G4 W abundances and G5 granites. **j** – Positive correlation with Bi and fractionation in G1-G2 granites and no overall trend in G3-G4 granites.

Fig. 5. Regional maps showing trace element distribution, subdivided by 50th, 75th, 90th, 95th, 99th and 100th percentiles for **a –** Li, **b** – Be, **c –** Ga, **d** – Nb, **e** – Ta, **f** – In, **g** – Sn, **h** – Sb, **I** – W and **j** – Bi. Note that high abundances for many of the metals are centred over the G5 granites of the Tregonning and St. Austell granites, with the exception of Be which has high abundances in G2 granites. Hemerdon, south of the Dartmoor Granite, shows high Sn, Sb, W and Bi and is most likely affected by subsolidus / hydrothermal processes.

Fig. 6. Lithium, Ga, Nb, Ta, In, Sn and W distribution shown as cumulative percent of whole rock abundances. **a** – Distribution for G1a granite. Gallium and Sn are fairly evenly distributed between major silicates. Indium and W are dominantly concentrated in muscovite, with Li, Nb and Ta in Mg siderophyllite. **b** – Distribution in G2 granite (with Li siderophyllite) is similar to G1a granite, with muscovite a dominant host for In and W and Li siderophyllite hosting Li and Nb. Note that Ta is depleted in major silicates, most likely partitioning into Fe-Ti oxides. **c** –Metal distribution in G2 granite (without Li siderophyllite). Niobium, Ta and Sn show depletions in major silicates and are again likely to be distributed in Fe-Ti oxides. Muscovite is again the dominant host of Nb, In and W, with Li partitioning into muscovite in the absence of trioctahedral micas. **d** –Other than W, the metals are accounted for in major silicates, particularly siderophyllite mica, in G3a granite, Land's End. Muscovite is an accessory mineral, fine-grained and subsolidus / late-stage and may represent a host of the metals, consistent with G1 and G2 granites. **e** – In G4b granite, St. Austell, Nb and Ta are strongly depleted in major silicates, most likely partitioning into rutile. Gallium is evenly distributed between major silicates whereas Li, In, Sn and W partition into zinnwaldite. **f** –Niobium, Ta, Sn, W and to some extent In, are depleted in major silicates, partitioning into accessory minerals such as rutile, ilmenite, cassiterite and wolframite in G5 granite, St. Austell.

Fig. 7. Model for G1-G2 granites: Combined 20% partial melting with 0% (i.e. only a 20% partial melt), 10% and 30% fractional crystallisation models for variable source abundances (x-axis) of the metals to account for source heterogeneity. The modelled abundances (y-axis) for a given source abundance are demonstrated by the symbols and the observed abundances for the Cornubian G1-G2

granites are on the right hand side. The average Gramscatho greywacke, taken as a proxy for the source, is indicated along with additional data from Devonian and Carboniferous shales from Hall (1990) and greywackes of Hu and Gao (2008) to show the possible ranges within sedimentary source material. For the majority of the elements, 30% partial melting and between 10 and 30% fractionation is sufficient to account for the range of abundances shown within the G1-G2 granites. There are notable exceptions. **b** – Be scatters upwards from modelled abundances, although these observed abundances may be achieved using higher source values of up to 5 ppm (London and Evensen, 2002). **c** – Ga partitions into plagioclase and micas and so modelled abundances do not significantly vary with fractionation. **h** – Modelled Sb abundances are significantly higher than observed Sb in the G1-G2 granites. This could be due to an overestimation of Sb in the source, partitioning into the residue during melting that is not accounted for by current partition coefficients or lack of magmatic control on Sb in SW England.

Fig. 8. Model for G3-G4 granites: Combined 30% partial melting with 0% (i.e. only a 20% partial melt), 10% and 30% fractional crystallisation models for variable source abundances (x-axis) of the metals to account for source heterogeneity. Other details remain the same as Fig. 6. **d** – Nb and **g** - Sn scatter towards higher observed abundances than those modelled using a Gramscatho greywacke source abundance, most likely attributable to variable partitioning of these elements facilitated by evolution of the melt towards high-F (see discussion) or overestimation of partitioning. The remaining metals are accounted for by 30% partial melting and 40% fractionation. As with G1-G2 granite models, modelled **h** – Sb abundances are significantly higher than those observed, again attributable to an overestimation of Sb incompatibility, partitioning into the residue during melting that is not accounted for by current partition coefficients or lack of magmatic control on Sb in SW England, with the latter most likely due to lack of correlation between Sb and magmatic evolution indicators such as $1/TiO_2$.

Fig. 9. Multi element plots showing partial melting models of a greywacke source, similar in composition to the Gramscatho Formation, to produce **a** – G1 two mica granite and **b** – G3 biotite

granite. The least evolved G1 and G3 granites were selected for modelling. For G1 granite, 20% partial melting is sufficient to attain the abundances of the majority of the metals observed, with the exception of Li, Nb, Sn and Sb. For G3 granites, 30% partial melting of a muscovite-depleted source, consistent with higher T melting, is sufficient to attain the observed concentrations, with the exception of Li and Sn. For both, the observed Li abundances could be attained with a higher source Li abundance and the compatibility of Sn is likely overestimated using the mineral/melt ratios from this study. Niobium partitioning is likely also controlled by Fe-Ti oxides and residual biotite during melting.

Fig. 10. Trace element variation diagrams using Mg (wt. %) as the abscissa showing G1-G4 granites, lamprophyre, basalt and mafic microgranular enclave (MME) data. These diagrams represent the typical trends for all trace elements in this study. **a** – Beryllium plot, showing converse trends for G1-G2 and G3-G4 granites, with mafic and ultramafic rocks and MME lying away from the granite trends, towards moderate to low Be abundances. **b** – Niobium plot showing the main granite trend, with mafic and ultramafic rocks and MME lying towards higher Nb abundances. It is not possible to decipher linear mixing lines through lamprophyres, basalts, MME and granites, implying that magma mixing is not a dominant factor in controlling metal distribution.

Fig. 11. Nb/Ta vs. Ta. G1-G2 granites show a curvilinear trend for both elements, typical of fractionation. For G3-G4 granites, Ta shows a curvilinear trend, typical of fractionation,. G5 granites plot towards high Ta abundances. The proposed value of Nb/Ta < 5 for the magmatic-hydrothermal transition in peraluminous granites (Ballouard et al., 2016) indicates the majority of the samples lie in the authors defined magmatic field, consistent with field and other geochemical observations.

Fig. 12. Trace element variation diagrams with P_2O_5 (wt. %) as the abscissa. P_2O_5 becomes concentrated in residual fluids during evolution of peraluminous granites and positive correlations for **a** – Sn and **b** – In indicate these metals may also be concentrated in residual fluids. The G2 granite outlier with low P_2O_5 is Hemerdon, most likely affected by subsolidus / hydrothermal processes.

Fig. 13. Trace element variation diagrams for trioctahedral (biotite) micas with Mg-Li (apfu) as the abscissa. With granite evolution, Mg decreases and Li increases, resulting in decreasing Mg-Li value. **a** W increases with granite evolution, showing strong enrichment in lepidolite and zinnwaldite micas. **b** – Nb decreases with granite evolution, although increases in whole rock data. This is due to increased F in evolved granites promoting the retention of Nb in the melt and consequential partitioning into accessory minerals on crystallisation of an F-bearing mineral such as topaz (e.g. Linnen, 1998), see also Fig. 9. **c** – In and **d** – Ga increase towards zinnwaldite before decreasing in lepidolite. This may represent the effects of F, or variable partitioning of these elements during source melting of the topaz granites.

Tables

Table 1. Mean Li, Be, Ga, Nb, Ta, In, Sn, Sb, W and Bi (in ppm, In in ppb) in the Cornubian Batholith relative to the average crustal values of Rudnick and Gao (2004) and average greywacke and shales of Hu and Gao (2008). Full data are provided in Supplementary Table 1.

Table 2. Samples, representative of the mineralogical diversity within the Cornubian Batholith, analysed by LA-ICP-MS and their constituent mineralogy.

Table 3. Mean abundance of Li, Ga, Nb, Ta, In, Sn and W in major silicate minerals in G1-G5 granites of the Cornubian Batholith (ppm). Full data are provided in Supplementary Table 2.

Supplementary Data

Supplementary Table 1. All bulk rock geochemical data and grid references for sampling locations with standard reference material data.

Supplementary Table 2. Spreadsheet with complete EPMA and LA-ICP-MS data for G1-G5 granites with BCR-2G and NIST-612 recoveries.

Supplementary Table 3. Modelling results for G1-G2 granites.

Supplementary Table 4. Modelling results for G3-G4 granites.

Supplementary Fig. 1: Additional modelling plot: Multi-element plots showing fractional crystallisation models for fractionation of the assemblages described in text from the least to the most evolved granites in the **a** – G1-G2 granites and **b** – G3-G4 granites. For G1-G2 granites, there is a good match for the majority of the metals with 30% fractionation. Note that Sb was below detection in the most evolved G2 sample. For G3-G4 granites, 40% fractionation is consistent with a number of the metals, with the exception of Li, which has a higher observed abundance than modelled, and Be and Sb which have lower observed abundances than modelled.

Supplementary Fig. 2. Correlation between F (wt. %) and Nb (ppm) in trioctahedral micas. This also represents the decrease in Nb in micas with decreasing Mg and increasing Li from Mg siderophyllite (G1/G3) through to lepidolite (G5). The decrease of Nb in G4 and G5 granites supports partitioning of Nb into accessory minerals, most likely Fe-Ti oxides (see also Fig. 5) and demonstrates the importance of high F in promoting high HFSE in peraluminous melts (e.g. Linnen, 1998).

References

Adam, J., Green, T., 2006. Trace element partitioning between mica- and amphibole-bearing garnet lherzolite and hydrous basanitic melt 1: Experimental results and the investigation of controls on partitioning behaviour. Contributions to Mineralogy and Petrology 152, 1-17.
Alderton, D.H.M., Moore, F., 1981. New determinations of tin and tungsten in granites from south-west England. Mineralogical Magazine 44, 354-356.
Alderton, D.H.M., Pearce, J.A., Potts, P.J., 1980. Rare earth element mobility during granite alteration: evidence from southwest England. Earth and Planetary Science Letters 49, 149-165.
Alexander, A.C., Shail, R.K., 1995. Late Variscan structures on the coast between Perranporth and St. Ives, Cornwall. Proceedings of the Ussher Society 8, 398-404.

Andersen, J.C.Ø., Stickland, R.J., Rollinson, G.K., Shail, R.K., 2016. Indium mineralisation in SW England: Host parageneses and mineralogical relations. Ore Geology Reviews 78, 213-238.
Ballouard, C., Poujol, M., Boulvais, P., Branquet, Y., Tartèse, R., Vigneresse, J.L., 2016. Nb-Ta fractionation in peraluminous granites: A marker of the magmatic-hydrothermal transition. Geology 44, 231-234.
Bea, F., Pereira, M.D., Corretgé, L.G., Fershtater, G.B., 1994. Differentiation of strongly peraluminous, perphosphorus granites: The pedrobernardo pluton, central Spain. Geochimica et Cosmochimica Acta 58, 2609-2627.
Belkasmi, M., Cuney, M., Pollard, P.J., Bastoul, A., 2000. Chemistry of the Ta-Nb-Sn-W oxide minerals from the Yichun rare metal granite (SE China): genetic implications and comparison with Moroccan and French Hercynian examples. Mineralogical Magazine 64.
Breiter, K., 2012. Nearly contemporaneous evolution of the A- and S-type fractionated granites in the Krušné hory / Erzegebirge Mts., Central Europe. Lithos 151, 105-121.
Breiter, K., 2014. Trace element composition of quartz from different types of pegmatites: A case study from the Moldanubian Zone of the Bohemian Massif (Czech Republic). Mineralogical Magazine 78, 703-722.
Breiter, K., Frýda, J., Seltmann, R., Thomas, R., 1997. Mineralogical Evidence for Two Magmatic Stages in the Evolution of an Extremely Fractionated P-rich Rare-metal Granite: the Podlesí Stock, Krušné Hory, Czech Republic. Journal of Petrology 38, 1723-1739.
Breiter, K., Gardenova, N., Vaculovic, T., Kanicky, V., 2013. Topaz as an important host for Ge in granites and greisens. Mineralogical Magazine 77, 403-417.
Breiter, K., Müller, A., Leichmann, J., Gabasova, A., 2005. Textural and chemical evolution of a fractionated granitic system: the Podlesi stock, Czech Republic. Lithod 80, 323-345.
Černý, P., Belvin, P.L., Cuney, M., London, D., 2005. Granite-related ore deposits. Economic Geology 100th Anniversary Volume, 337-370.
Chappell, B.W., 1996. Magma mixing and the production of compositional variation within granite suites: Evidence from the granites of southeastern Australia. Journal of Petrology 37, 449-470.
Chappell, B.W., Hine, R., 2006. The Cornubian Batholith: an example of magmatic fractionation on a crustal scale. Resource Geology 56, 203-244.
Charoy, B., 1986. The genesis of the Cornubian Batholith (South-West England): the example of the Carnmenellis Pluton. Journal of Petrology 27, 571-604.
Chen, Y., Clark, A.H., Farrar, E., Wasteneys, H.A.P., Hodgson, M.J., Bromley, A.V., 1993. Diachronous and independent histories of plutonism and mineralisation in the Cornubian Batholith, southwest England. Journal of the Geological Society 150, 1183-1191.
Chesley, J.T., Halliday, A.N., Snee, L.W., Mezger, K., Shepherd, T.J., Scrivener, R.C., 1993. Thermochronology of the Cornubian Batholith in southwest England: Implications for pluton emplacement and protracted hydrothermal mineralisation. Geochimica et Cosmochimica Acta 57, 1817-1835.
Clark, A.H., Chen, Y., Farrar, E., B., N., 1994. Refinement of the time-space relationships of intrusion and hydrothermal activity in the Cornubian Batholith [Abstract only]. Proceedings of the Ussher Society, 345.
Clayton, R.E., Spiro, B., 2000. Sulphur, carbon and oxygen isotope studies of early Variscan mineralisation and Pb-Sb vein deposits in the Cornubian Orefield: implications for the scale of fluid movements during Variscan deformation. Mineralium Deposita 35, 315-331.
Cook, N.J., Ciobanu, C.L., Pring, A., Skinner, W., Shimizu, M., Danyushevsky, L., Saini-Eidukat, B., Melcher, F., 2009. Trace and minor elements in sphalerite: A LA-ICPMS study. Geochimica et Cosmochimica Acta 73, 4761-4791.
Cook, N.J., Ciobanu, C.L., Williams, T., 2011a. The mineralogy and mineral chemistry of indium in sulphide deposits and implications for mineral processing. Hydrometallurgy 108, 226-228.

Cook, N.J., Sundblad, K., Valkama, M., Nygård, R., Ciobanu, C.L., Danyushecsky, L., 2011b. Indium mineralisation in A-type granites in southeastern Finland: Insights into mineralogy and partitioning between coexisting minerals. Chemical Geology 284, 62-73.
Cuney, M., Barbey, P., 2014. Uranium, rare metals and granulite-facies metamorphism. Geoscience Frontiers, 1-17.
Dangerfield, J., Hawkes, J.R., 1981. The Variscan granites of south-west England: additional information. Proceedings of the Ussher Society 5, 116-120.
Darbyshire, D.P.F., Shepherd, T.J., 1985. Chronology of granite magmatism and associated mineralisation, SW England. Journal of the Geological Society 142, 1159-1177.
Darbyshire, D.P.F., Shepherd, T.J., 1994. Nd and Sr isotope constraints of the origin of the Cornubian Batholith, SW England. Journal of the Geological Society 151, 795-802.
Drivenes, K., Larsen, R., Müller, A., Sørensen, B., Wiedenbeck, M., Raanes, M., 2015. Late-magmatic immiscibility during batholith formation: assessment of B isotopes and trace elements in tourmaline from the Land's End granite, SW England. Contributions to Mineralogy and Petrology 169, 1-27.
Drivenes, K., Larsen, R.B., Müller, A., Sørensen, B.E., 2016. Crystallization and uplift path of late Variscan granites evidenced by quartz chemistry and fluid inclusions: Example from the Land's End granite, SW England. Lithos 252-253, 57-75.
Dupuis, N.E., Braid, J.A., Murphy, J.B., Shail, R.K., Archibald, D.A., Nance, R.D., 2015. 40Ar/39Ar phlogopite geochronology of lamprophyre dykes in Cornwall, UK: new age constraints on Early Permian post-collisional magmatism in the Rhenohercynian Zone, SW England. Journal of the Geological Society 172, 566.
European Commision, 2014. Report of critical raw materials for the EU: report of the ad hoc working group on defining critical raw materials. European Commission, Belgium.
Evensen, J.M., London, D., 2003. Experimental partitioning of Be, Cs, and other trace elements between cordierite and felsic melt, and the chemical signature of S-type granite. Contributions to Mineralogy and Petrology 144, 739-757.
Ewart, A., Griffin, W.L., 1994. Application of proton-microprobe data to trace-element partitioning in volcanic rocks. Chemical Geology 117, 251-284.
Exley, C.S., Stone, M., 1964. The granitic rocks of south-west England, in: Hosking, K.F.G., Shrimpton, G.J. (Eds.), Present views of some aspects of the geology of Cornwall and Devon. Royal Geological Society of Cornwall, Penzance, pp. 131-184.
Exley, C.S., Stone, M., 1982. Hercynian intrusive rocks, in: Sutherland, D.S. (Ed.), Igneous rocks of the British Isles. John Wiley & Sons, Chichester, pp. 287-320.
Floyd, P.A., Shail, R., Leveridge, B.E., Franke, W., 1991. Geochemistry and provenance of Rhenohercynian synorogenic sandstones: implications for tectonic environment discrimination. Geological Society, London, Special Publications 57, 173-188.
Förster, H.-J., Tischendorf, G., Trumbull, R.B., Gottesmann, B., 1999. Late-collisional granites in the Variscan Erzgebirge, Germany. Journal of Petrology 40, 1613-1645.
Franke, W., 2000. The mid-European segment of the Variscides: tectonostratigraphic units, terrane boundaries and plate tectonic evolution. Geological Society, London, Special Publications 179, 35-61.
Ghosh, P.K., 1927. Petrology of the Bodmin Moor Granite (eastern part), Cornwall. Mineralogical Magazine 21, 285-309.
Gomes, M.E.P., Neiva, A.M.R., 2002. Petrogenesis of tin-bearing granites from Ervedosa, Northern Portugal: The importance of magmatic processes. Chemie der Erde - Geochemistry 62, 47-72.
Haapala, I., 1997. Magmatic and postmagmatic processes in tin-mineralized granites: Topaz-bearing leucogranite in the Eurajoki Rapakivi Granite Stock, Finland. Journal of Petrology 38, 1645-1659.
Haapala, I., Lukkari, S., 2005. Petrological and geochemical evolution of the Kymi stock, a topaz granite cupola within the Wiborg rapakivi batholith, Finland. Lithos 80, 347-362.
Hall, A., 1971. Greisenisation in the granite of Cligga Head, Cornwall. Proceedings of the Geologist's Association 82, 209-230.
Hall, A., 1990. Geochemistry of the Cornubian tin province. Mineralium Deposita 25, 1-6.

Harris, N., Ayres, M., Massey, J., 1995. Geochemistry of granitic melts produced during the incongruent melting of muscovite: implications for extraction of Himalayan leucogranite magmas. Journal of Geophysical Research 100, 15767-15777.
Harris, N.B.W., Inger, S., 1992. Trace element modelling of pelite-derived granites. Contributions to Mineralogy and Petrology 110, 46-56.
Henderson, C.M.B., Martin, J.S., Mason, R.A., 1989. Compositional relations in Li-micas from SW England and France: an ion- and electron-microprobe study. Mineralogical Magazine 53, 427-449.
Hill, P.I., Manning, D.A.C., 1987. Multiple intrusions and pervasive hydrothermal alteration in the St. Austell Granite, Cornwall. Proceedings of the Ussher Society 6, 447-453.
Hosking, K.F.G., 1954. The pegmatites of Trolvis Quarry, Carnmenellis, Cornwall. Geological Magazine 140, 273-285.
House of Commons, 2011. House of Commons Science and Technology Committee: Strategically important metals. House of Commons, London.
Hu, Z., Gao, S., 2008. Upper crustal abundances of trace elements: a revision and update. Chemical Geology 253, 205-221.
Huang, L.-C., Jiang, S.-Y., 2014. Highly fractionated S-type granites from the giant Dahutang tungsten deposit in Jiangnan Orogen, Southeast China: geochronology, petrogenesis and their relationship with W-mineralization. Lithos 202-203, 207-226.
Jackson, N.J., Willis-Richards, J., Manning, D.A.C., Sams, M.S., 1989. Evolution of the Cornubian Orefield, southwest England: Part II. Mineral deposits and ore-forming processes. Economic Geology 84, 1101-1133.
Jenner, F.E., O'Neill, H.S.C., 2012. Major and trace analysis of basaltic glasses by laser-ablation ICP-MS. Geochemistry, Geophysics, Geosystems 13, 1-17.
Jovic, S.M., Guido, D.M., Schalamuk, I.B., Ríos, F.J., Tassinari, C.C.G., Recio, C., 2011. Pingüino In-bearing polymetallic vein deposit, Deseado Massif, Patagonia, Argentina: characteristics of mineralization and ore-forming fluids. Mineralium Deposita 46, 257-271.
Keppler, H., 1993. Influende of fluorine on the enrichment of high field strength elements in granitic rocks. Contributions to Mineralogy and Petrology 114, 479-488.
Kováříková, P., Siebel, W., Jelínek, E., Štemprok, M., Kachlík, V., Holub, F.V., Blecha, V., 2007. Petrology, geochemistry and zircon age for redwitzite at Abertamy, NW Bohemian Massif (Czech Republic): tracing the mantle component in Late Variscan intrusions. Chemie der Erde - Geochemistry 67, 151-174.
Leat, P.T., Thompson, R.N., Morrison, M.A., Hendry, G.L., Trayhorn, S.C., 1987. Geodynamic significance of post-Variscan intrusive and extrusive potassic magmatism in SW England. Earth and Environmental Science Transactions of the Royal Society of Edinburgh 77, 349-360.
Lehmann, B., 1982. Metallogeny of Tin: Magmatic differentiation versus geochemical heritage. Economic Geology 77, 50-59.
Lehmann, B., 1987. Tin granites, geochemical heritage, magmatic differentiation. Geologische Rundschau 76, 177-185.
Lehmann, B., 1990. Lecture notes in Earth Sciences 32: Metallogeny of tin. Springer-Verlag, Berlin.
Leveridge, B.E., Hartley, A.J., 2006. The Variscan Orogeny: The development of Devonian / Carboniferous basins in SW England and South Wales, in: Brenchley, P.J., Rawson, P.F. (Eds.), The Geology of England and Wales (2nd Ed.). Geological Society of London, London, pp. 225-255.
Linnen, R., 1998. The solubility of Nb-Ta-Zr-Hf-W in granitic melts with Li and Li + F: Constraints for mineralisation in rare metal granites and pegmatites. Economic Geology 93, 1013-1025.
London, D., Evensen, J.M., 2002. Beryllium in Silicic Magmas and the Origin of Beryl-Bearing Pegmatites. Reviews in Mineralogy and Geochemistry 50, 445-486.
London, D., Manning, D.A.C., 1995. Chemical variation and significance of tourmaline from southwest England. Economic Geology 90, 495-519.

Lukkari, S., Thomas, R., Haapala, I., 2009. Crystallisation of the Kymi topaz granite stock within the Wiborg rapakivi granite batholith, Finland: Evidence from melt inclusions. The Canadian Mineralogist 47, 1359-1374.
Manning, D.A.C., Henderson, P., 1984. The behaviour of tungsten in granitic melt-vapour systems. Contributions to Mineralogy and Petrology 89, 286-293.
Manning, D.A.C., Hill, P.I., 1990. The petrogenetic and metallogenetic significance of topaz granite from the southwest England orefield, in: Stein, H.J., Hannah, J.L. (Eds.), Ore-bearing granite systems: petrogenesis and mineralizing processes. Geological Society of American Special Paper, pp. 51-69.
Manning, D.A.C., Hill, P.I., Howe, J.H., 1996. Primary lithological variation in the kaolinized St. Austell Granite, Cornwall, England. Journal of the Geological Society 153, 827-838.
Marignac, C., Cuney, M., 1999. Ore deposits of the French Massif Central: insight into the metallogenesis of the Variscan collision belt. Mineralium Deposita 34, 472-504.
Marks, M.A.W., Marschall, H.R., Schühle, P., Guth, A., Wenzel, T., Jacob, D.E., Barth, M., Markl, G., 2013. Trace element systematics of tourmaline in pegmatitic and hydrothermal systems from the Variscan Schwarzwald (Germany): The importance of major element composition, sector zoning, and fluid or melt composition. Chemical Geology 344, 73-90.
Marschall, H.R., Dohmen, R., Ludwig, T., 2013. Diffusion-induced fractionation of niobium and tantalum during continental crust formation. Earth and Planetary Science Letters 375, 361-371.
Merino, E., Villaseca, C., Orejana, D., Jeffries, T., 2013. Gahnite, chrysoberyl and beryl co-occurrence as accessory minerals in a highly evolved peraluminous pluton: The Belvís de Monroy leucogranite (Cáceres, Spain). Lithos 179, 137-156.
Miroshnichenko, L.A., 1965. New data on distribution of indium in ore deposits of Central Kazakhstan. International Geology Review 7, 233-240.
Moore, J.M., Jackson, N.J., 1977. Structure and mineralisation in the Cligga Granite stock. Journal of the Geological Society 133, 467-480.
Moss, R.L., Tzimas, E., Kara, H., Willis, P., Kooroshy, J., 2011. Critical metals in strategic energy technologies. Institute for Energy and Transport, European Commission., Luxembourg.
Müller, A., Halls, C., 2005. Rutile - the tin-tungsten host in the intrusive tourmaline breccia at Wheal Remfry, SW England. Mineral Deposit Research: Meeting the Global Challenge, 441-444.
Müller, A., Seltmann, R., 1999. The genetic significance of snowball quartz in highly fractionated tin granites of the Krušné hory/Erzgebirg., in: Stanley, C.J. (Ed.), Proceedings of the Fifth Biennial SGA Meeting and the Tenth Quadrennial IAGOD Symposium: Mineral Deposits: Processes to Processing., London, pp. 409-412.
Müller, A., Seltmann, R., Halls, C., Siebel, W., Dulski, P., Jeffries, T., Spratt, J., Kronz, A., 2006. The magmatic evolution of the Land's End pluton, Cornwall, and associated pre-enrichment of metals. Ore Geology Reviews 28, 329-367.
Nance, R.D., Neace, E.R., Braid, J.A., Murphy, B., Dupuis, N., Shail, R.K., 2015. Does the Meguma Terrane extnd into SW England? Journal of the Geological Association of Canada 42, 61-76.
Neiva, A.M.R., 1987. Geochemistry of white micas from Portuguese tin and tungsten deposits. Chemical Geology 63, 299-317.
Neiva, A.M.R., Silva, M.M.V.G., Gomes, M.E.P., Campos, T.F.C., 2002. Geochemistry of coexisting biotite and muscovite of Portuguese peraluminous granitic differentiation series. Chemie der Erde - Geochemistry 62, 197-215.
Neves, L.J.P.F., 1997. Trace element content and partitioning between biotite and muscovite of granitic rocks: a study in the Viseu region (Central Portugal). European Journal of Mineralogy 9, 849-857.
Orsini, J.-B., Cocirta, C., Zorphi, M.-J., 1991. Genesis of mafic microgranular enclaves through differentiation of basic magmas, mingling and chemical exchanges with their host granitoid magmas, in: Dider, J., Barbarin, B. (Eds.), Developments in Petrology 13: Enclaves and granite petrology. Elsevier, Netherlands, pp. 445-464.

Perugini, D., De Campos, C.P., Dingwell, D.B., Poli, G., 2008. Trace element mobility during magma mixing: Preliminary experimental results. Chemical Geology 256, 146-157.
Pollard, P.J., Pichavant, M., Charoy, B., 1987. Contrasting evolution of fluorine- and boron-rich tin systems. Mineralium Deposita 22, 315-321.
Raimbault, L., Cuney, M., Azencott, C., Duthou, J.L., Joron, J.L., 1995. Geochemical evidence for a multistage magmatic genesis of Ta-Sn-Li mineralisation in the granite at Beauvoir, French Massif Central. Economic Geology 90.
Romer, R., Kroner, U., 2014. Sediment and weathering control on the distribution of Paleozoic magmatic tin–tungsten mineralization. Mineralium Deposita 50, 327-338.
Romer, R.L., Kroner, U., 2016. Phanerozoic tin and tungsten mineralization—Tectonic controls on the distribution of enriched protoliths and heat sources for crustal melting. Gondwana Research 31, 60-95.
Romer, R.L., Meixner, A., Förster, H.-J., 2014. Lithium and boron in late-orogenic granites - isotopic fingerprints for the source of crustal melts? Geochimica et Cosmochimica Acta 131, 98-114.
Rudnick, R.L., Gao, S., 2004. Composition of the Continental Crust, in: Holland, H.D., Turekian, K.K. (Eds.), Treatise on Geochemistry. Elsevier, Amsterdam, pp. 1-64.
Scott, P.W., Pascoe, R.D., Hart, F.W., 1998. Columbite-tantalite, rutile and other accessory minerals from the St Austell topaz granite, Cornwall. Geoscience in southwest England 9, 165-170.
Scrivener, R.C., 2006. Cornubian granites and mineralisation of SW England, in: Brenchley, P.J., Rawson, P.F. (Eds.), The Geology of England and Wales (2nd Ed.). Geological Society of London, London, pp. 257-268.
Seifert, T., 2008. Metallogeny and petrogenesis of lamprophyres in the Mid-European Variscides. IOS Press BV, Netherlands.
Selwood, E.B., Thomas, J.M., Williams, B.J., Clayton, R.E., Durning, B., Smith, O., Warr, L.N., 1998. Geology of the country around Trevose Head and Camelford: Memoir of the British Geological Survey, Sheets 335 and 336. British Geological Survey, United Kingdom.
Shail, R.K., Leveridge, B.E., 2009. The Rhenohercynian passive margin of SW England: Development, inversion and extensional reactivation. C.R. Geoscience 341, 140-155.
Shail, R.K., Stuart, F.M., Wilkinson, J.J., Boyce, A.J., 2003. The role of post-Variscan extensional tectonics and mantle melting in the generation of the lower Permian granites and giant W-As-Sn-Cu-Zn-Pb orefield of SW England. Transactions of the Institution of Mining and Metallogeny Section B: Applied Earth Science 112, 127-129.
Shail, R.K., Wilkinson, J.J., 1994. Late-to post-Variscan extensional tectonics in south Cornwall. Proceedings of the Ussher Society 8, 262-270.
Sial, A.N., Bettencourt, J.S., De Campos, C.P., Ferreira, V.P., 2011. Granite-related ore deposits: an introduction. Geological Society, London, Special Publications 350, 1-5.
Simons, B., Shail, R.K., Andersen, J.C.Ø., 2016. The petrogenesis of the Early Permian Variscan granites of the Cornubian Batholith – lower plate post-collisional peraluminous magmatism in the Rhenohercynian Zone of SW England. Lithos 260, 76-94.
Spear, F.F., Kohn, M.J., Cheney, J.T., 1999. P-T paths from anatectic pelites. Contributions to Mineralogy and Petrology 134, 17-32.
Stampfli, G.M., Hochard, C., Vérard, C., Wilhem, C., vonRaumer, J., 2013. The formation of Pangea. Tectonophysics 593, 1-19.
Štemprok, M., 1987. Greisenization (a review). Geologische Rundschau 76, 169-175.
Štemprok, M., Seifert, T., 2010. The association of lamprophyric intrusions and rare-metal mineralisation. Mineralogia Special Papers 37, 61-62.
Stepanov, A., Mavrogenes, J.A., Meffre, S., Davidson, P., 2014. The key role of mica during igneous concentration of tantalum. Contributions to Mineralogy and Petrology 167, 1009-1016.
Stepanov, A.S., Hermann, J., 2013. Fractionation of Nb and Ta by biotite and phengite: implications for the "missing Nb paradox". Geology 41, 303-306.

Stimac, J.A., Clark, A.H., Chen, Y., Garcia, S., 1995. Enclaves and their bearing on the origin of the Cornubian Batholith, southwest England. Mineralogical Magazine 59, 273-296.
Stone, M., 1975. Structure and petrology of the Tregonning-Godolphin Granite, Cornwall. Proceedings of the Geologist's Association 86, 155-170.
Stone, M., 1992. The Tregonning Granite: petrogenesis of Li-mica granites in the Cornubian Batholith. Mineralogical Magazine 56, 141-155.
Stone, M., Exley, C.S., George, M.C., 1988. Compositions of trioctahedral micas in the Cornubian Batholith. Mineralogical Magazine 52, 175-192.
Stone, M., George, M.C., 1978. Amblygonite in leucogranites of the Tregonning-Godolphin Granite, Cornwall. Mineralogical Magazine 42, 151-152.
Stone, M., George, M.C., 1983. Some phosphate minerals at the Megiliggar Rocks, Cornwall. Proceedings of the Ussher Society 5, 428-431.
Taylor, J.R., Wall, V.J., 1992. The behaviour of tin in granitoid magmas. Economic Geology 87, 403-420.
Teixeira, R.J.S., Neiva, A.M.R., Gomes, M.E.P., Corfu, F., Cuesta, A., Croudace, I.W., 2012. The role of fractional crystallization in the genesis of early syn-D3, tin-mineralized Variscan two-mica granites from the Carrazeda de Ansiães area, northern Portugal. Lithos 153, 177-191.
Tindle, A.G., 1991. Trace element behaviour in microgranular enclaves from granitic rocks, in: Dider, J., Barbarin, B. (Eds.), Deveopments in Petrology 13: Enclaves and granite petrology. Elsevier, Netherlands.
Tischendorf, G., Förster, H.-J., Gottesmann, B., 2001. Minor- and trace-element composition of trioctahedral micas: a review. Mineralogical Magazine 65, 249-276.
Tischendorf, G., Gottesmann, B., Forster, H.-J., Trumbull, R.B., 1997. On Li-bearing micas: estimating Li from electron microprobe analyses and an improved diagram for graphical representation. Mineralogical Magazine 61, 809-834.
Warr, L.N., Primmer, T.J., Robinson, D., 1991. Variscan very low-grade metamorphism in southwest England: a diastathermal and thrust-related origin. Journal of Metamorphic Geology 9, 751-764.
White, S.J.O., Keach, C., Hemond, H.F., 2015. Atmospheric deposition of indium in the Northeastern United States: Flux and historical trends. Environmental Science and Technology 49, 12705-12713.
Williamson, B.J., Müller, A., Shail, R.K., 2010. Source and partitioning of B and Sn in the Cornubian Batholith of southwest England. Ore Geology Reviews 38, 1-8.
Williamson, B.J., Stanley, C.J., Wilkinson, J.J., 1997. Implications from inclusions in topaz for greisenisation and mineralisation in the Hensbarrow topaz granite, Cornwall, England. Contributions to Mineralogy and Petrology 127, 119-128.
Willis-Richards, J., Jackson, N.J., 1989. Evolution of the Cornubian ore field, southwest England: Part I. Batholith modeling and ore distribution. Economic Geology 84, 1078-1100.
Yu, Z., Robinson, P., McGoldrick, P., 2001. An evaluation of methods for the chemical decomposition of geological materials for trace element determination using ICP-MS. Geostandards Newsletter 25, 199-217.

Table 1

		Li	Be	Ga	Nb	Ta	In*	Sn	Sb	W	Bi
Detection limt (ppm)	n	1	0.1	5	0.3	0.3	25	0.2	0.02	1	0.06
G1a	23	252	6.5	26	11	2.2	41	11	0.27	3.9	0.44
G1b	8	290	9.5	26	11	1.9	51	12	0.28	3.3	0.39
G1c	6	108	4.0	23	14	1.7	27	5.2	0.31	1.9	0.23
G2**	9	315	12	24	16	4.4	74	18	0.16	12	0.46
G3a	26	231	5.4	23	17	2.8	55	12	0.44	5.7	0.40
G3c	4	158	5.0	19	15	2.7	31	10	0.29	5.8	0.21
G4a	11	219	2.1	27	22	3.6	87	14	0.22	3.4	0.24
G4b	5	445	4.8	28	29	4.9	74	14	0.37	6.8	0.57
G4c	7	273	3.2	28	24	4.5	90	13	0.14	7.2	0.94
G4d	3	128	2.3	-	18	2.2	31	7.6	b.d.	2.2	b.d.
G5a	7	1363	3.5	38	52	15	47	21	0.36	24	0.82
G5b	2	2467	8.8	40	54	14	40	8.1	0.78	25	0.52
Gramscatho[+]	4	40	2.2	16	9.2	1.1	44	1.9	0.63	n/a	0.16
Average upper crust[1]	-	24	2.1	17.5	12	0.9	56	2.1	0.40	1.9	0.16
Average lower crust[1]	-	13	1.4	13	5	0.6	50	1.7	0.10	0.6	0.20
Greywacke[2]	4	44	2	19	15	1.1	73	3.5	0.52	1.5	0.27
Shale[2]	11	63	4	23	18	1.5	88	4.5	0.77	2.7	0.54

*Indium data in ppb. **Hemerdon is omitted due to hydrothermal alteration. [1]From Rudnick and Gao (2004); [2]Averaged from Hu and Gao (2008). [+]Ground samples (GG6, GG15, GG28, GG44) sourced from the study of Darbyshire and Shepherd (1994). Tungsten not analysed due to sample preparation method. Included in this table are samples from Natural History Museum collection BM.2004,P14: G3a- specimen numbers 7, 24, 30; G4a - specimen number 8; G4c - specimen numbers 1, 31; G4d - specimen numbers 10, 21, 23.

Table 2.

Sample	Type	Pluton	Major silicate minerals
CN09	G1a	Carnmenellis	Qtz, Kfs, Pl (An_{17}), Msc, FeMsc, Mg Sid, Tur
CL02	G2	Cligga	Qtz, Kfs, Pl (An_{5}), Msc, FeMsc, Li Sid, Tur
KT01	G2	Kit Hill	Qtz, Kfs, Pl (An_{7}), Msc, Tur
LE08	G2	Land's End	Qtz, Kfs, Pl (An_{1}), Msc, FeMsc, Li Sid, Tur
LE02	G3a	Land's End	Qtz, Kfs, Pl (An_{10}), Mg Sid, Crd, Tur
DT07	G3a	Dartmoor	Qtz, Kfs, Pl (An_{14}), Sid, Tur
AU12	G4a	St. Austell	Qtz, Kfs, Pl (An_{1}), Zwd, Tur
AU06	G5	St. Austell	Qtz, Kfs, Pl (An_{1}), Poly, Tz

Abbreviations: Crd – Cordierite; FeMsc – Ferroan muscovite; Kfs – Alkali feldspar (orthoclase); Li Sid – Lithian siderophyllite; Mg Sid – Magnesian siderophyllite; Msc – Muscovite; Pl – Plagioclase; Poly – Polylithionite; Qtz – Quartz; Sid – Siderophyllite; Tur – Tourmaline (schorl); Tz – Topaz; Zwd – Zinnwaldite

Table 3

		Li	Ga	Nb	Ta	In	Sn	W
Detection limt (ppm)		0.15	0.08	0.02	0.01	0.01	0.10	0.03
G1	**n**							
Mg siderophyllite	9	3097	95	149	10	0.20	34	3.8
Muscovite	3	1250	157	66	7.8	1.13	58	64
Ferroan muscovite	6	1547	140	58	11	1.10	66	82
Plagioclase (oligoclase)	10	34	34	0.30	0.09	0.02	8.6	0.05
Orthoclase	8	11	21	0.81	0.03	b.d.	13	0.05
Tourmaline	11	120	145	0.94	0.66	0.27	8.5	0.16
G2								
Li siderophyllite	7	6070	114	188	9.7	0.31	53	20
Muscovite	10	2379	118	115	20	0.74	65	94
Ferroan muscovite	15	3034	119	139	22	0.60	63	124
Plagioclase (albite)	11	56	39	0.59	0.11	0.06	19	0.58
Orthoclase	15	65	42	0.88	1.10	0.12	15	0.27
Tourmaline	15	210	120	2.6	1.6	0.20	10	0.07
G3								
Mg siderophyllite	3	2085	90	43	16	0.28	34	8.9
Siderophyllite	13	3247	95	234	24	0.44	66	9.1
Plagioclase (oligoclase)	13	22	31	0.28	0.06	0.02	11	0.23
Orthoclase	10	9.5	18	0.04	0.02	0.05	13	0.91
Tourmaline	7	115	112	1.6	1.2	0.17	20	0.51
Cordierite	3	3857	47	0.18	0.02	0.02	5.7	0.19
G4								
Zinnwaldite	8	16299	105	109	11	1.1	111	163
Plagioclase (albite)	5	165	35	1.3	0.12	0.10	17	2.0
Orthoclase	1*	47	22	0.03	b.d.	0.08	14	0.27
Tourmaline	3	509	147	0.76	0.25	0.16	4.9	0.19
G5								
Lepidolite	7	22650	83	95	16	0.17	13	195
Plagioclase (albite)	6	23	46	0.56	0.19	0.03	9.5	1.1
Orthoclase	2*	16	35	0.10	0.02	0.03	8.8	0.20
Topaz	3	1.8	6.1	0.50	0.10	0.02	1.2	0.35

*Analyses affected by presence of microperthite.

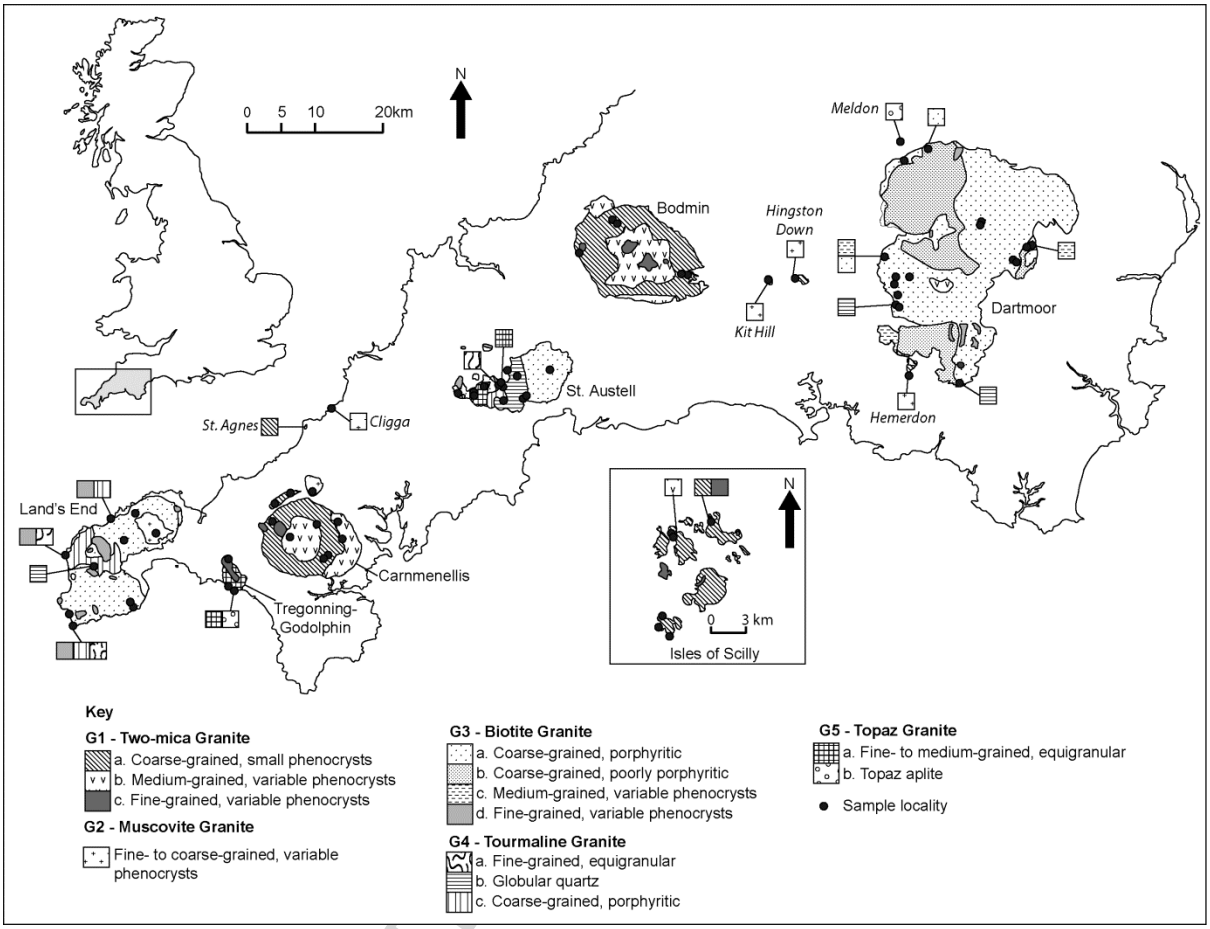

Figure 1

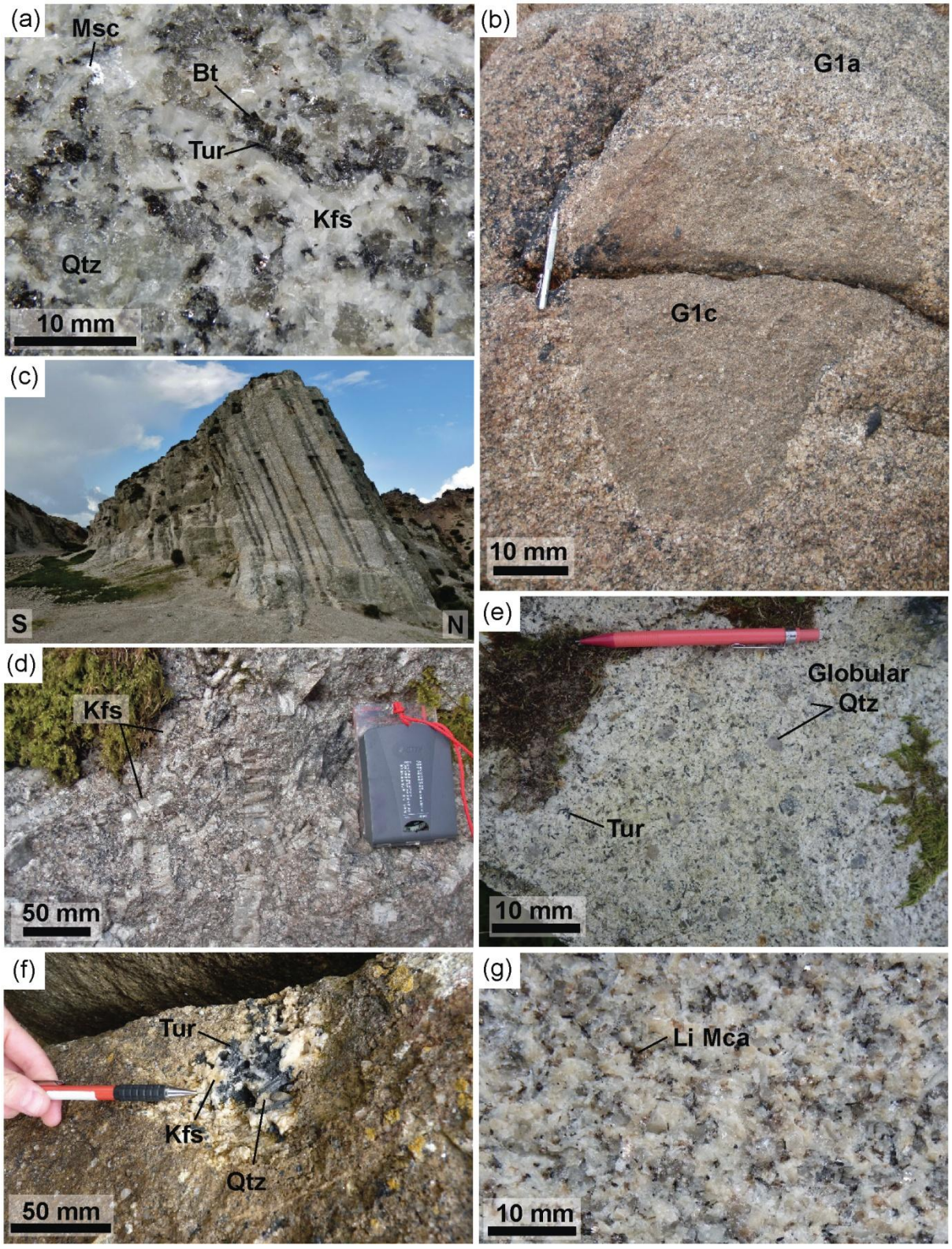

Figure 2

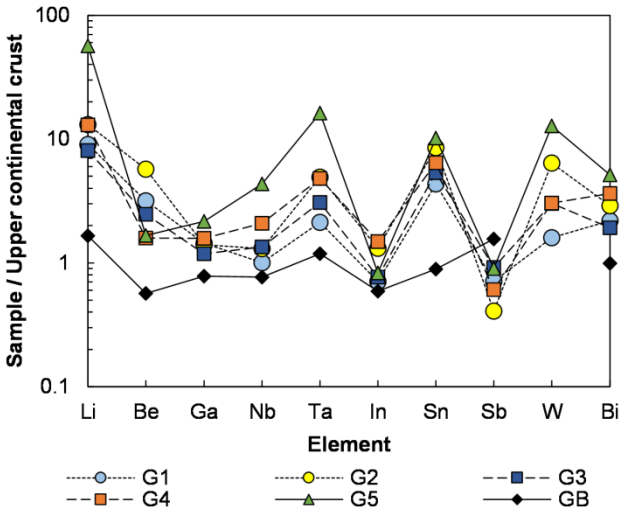

Figure 3

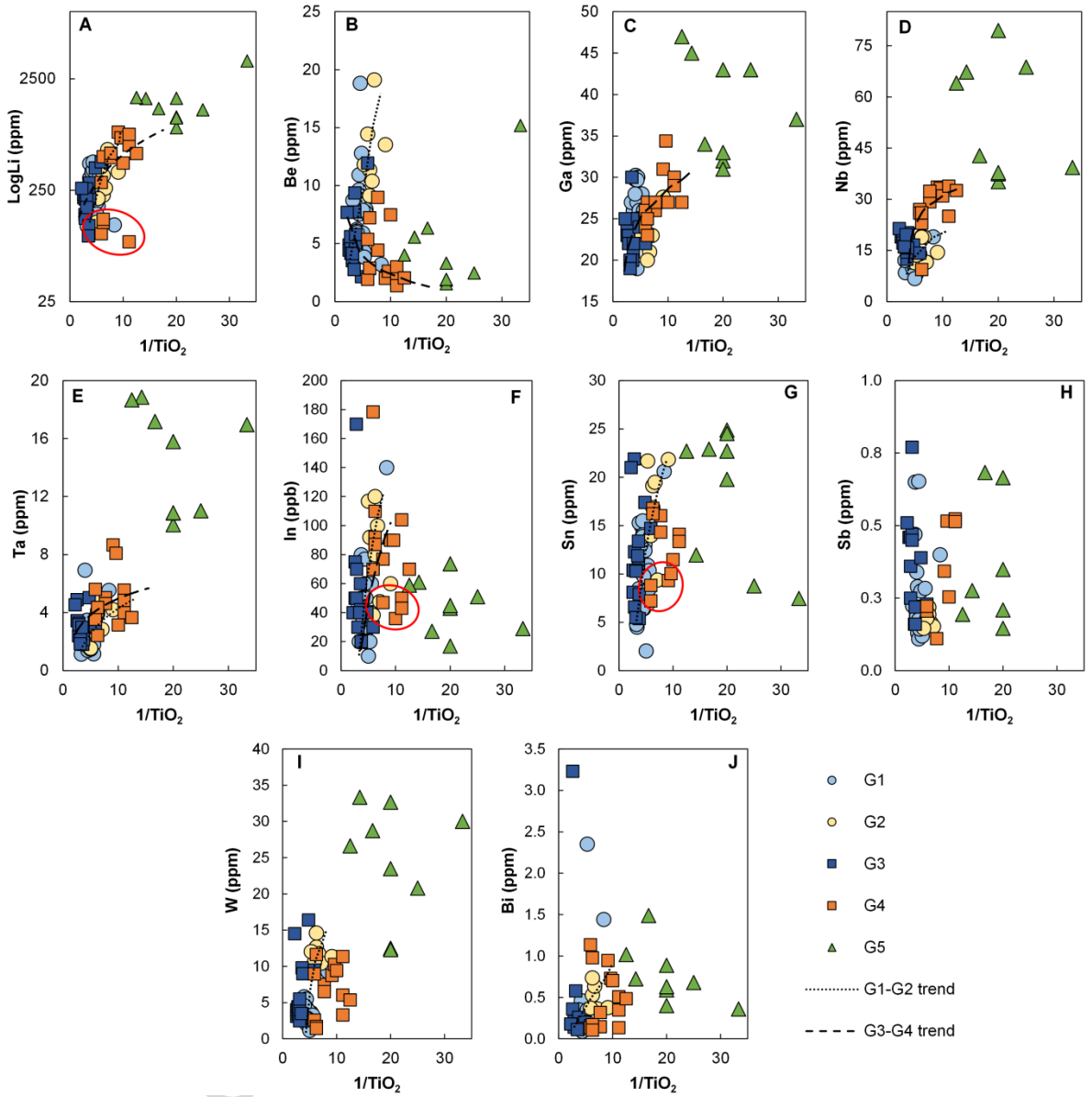

Figure 4

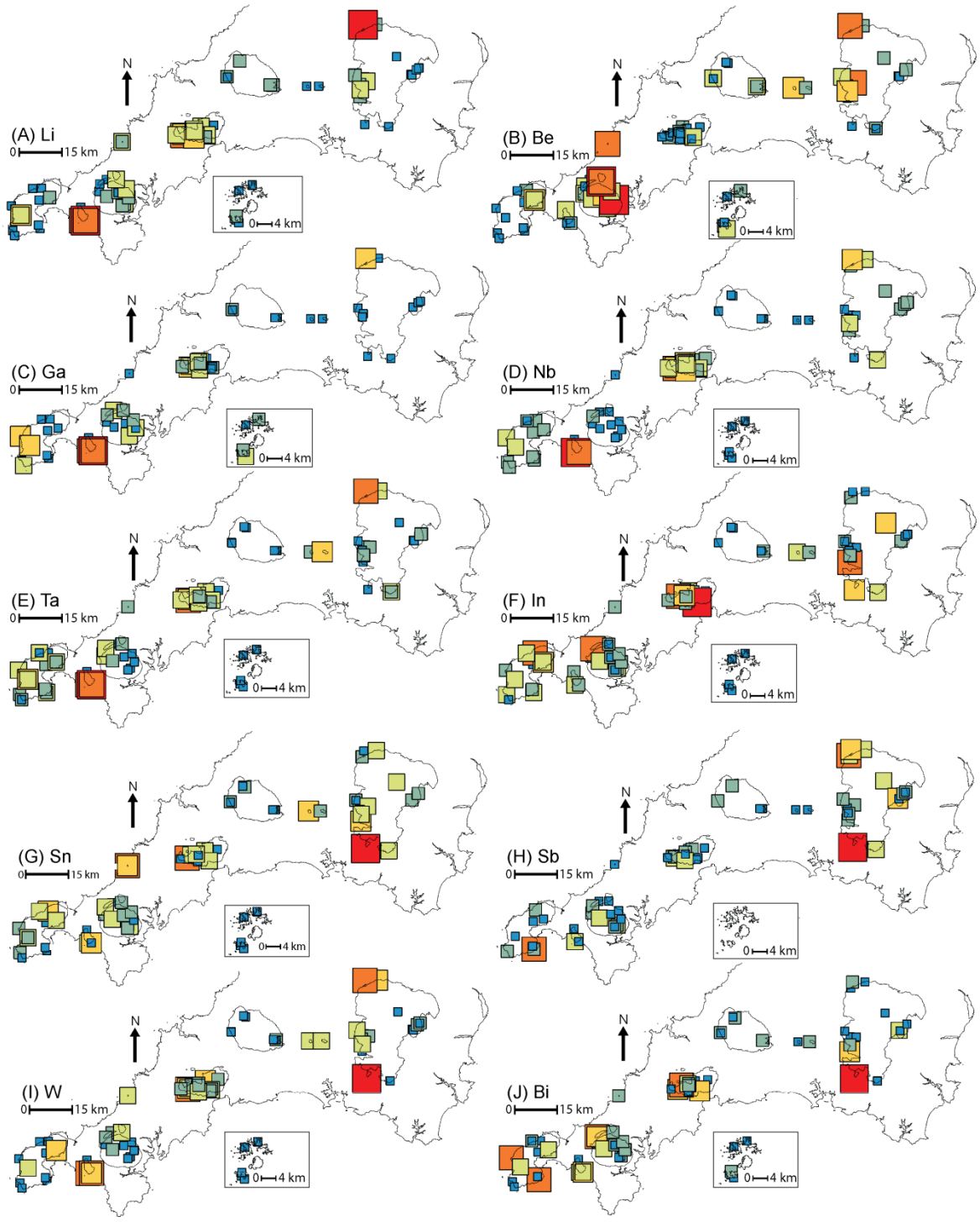

Percentile		Li	Be	Ga	Nb	Ta	In*	Sn	Sb	W	Bi
50th		257	5.4	26	16	2.6	45	12	0.28	5	0.35
75th		394	8.3	28	21	4.3	70	15	0.45	10	0.56
90th		770	11.2	33	35	8.4	98	21	0.65	14	1.01
95th		1279	13.0	40	41	11.0	120	23	0.77	26	1.65
99th		1698	18.7	45	69	18.6	169	25	1.37	33	3.43
100th		3619	19.1	47	79	18.9	178	35	2.13	64	6.16

Figure 5

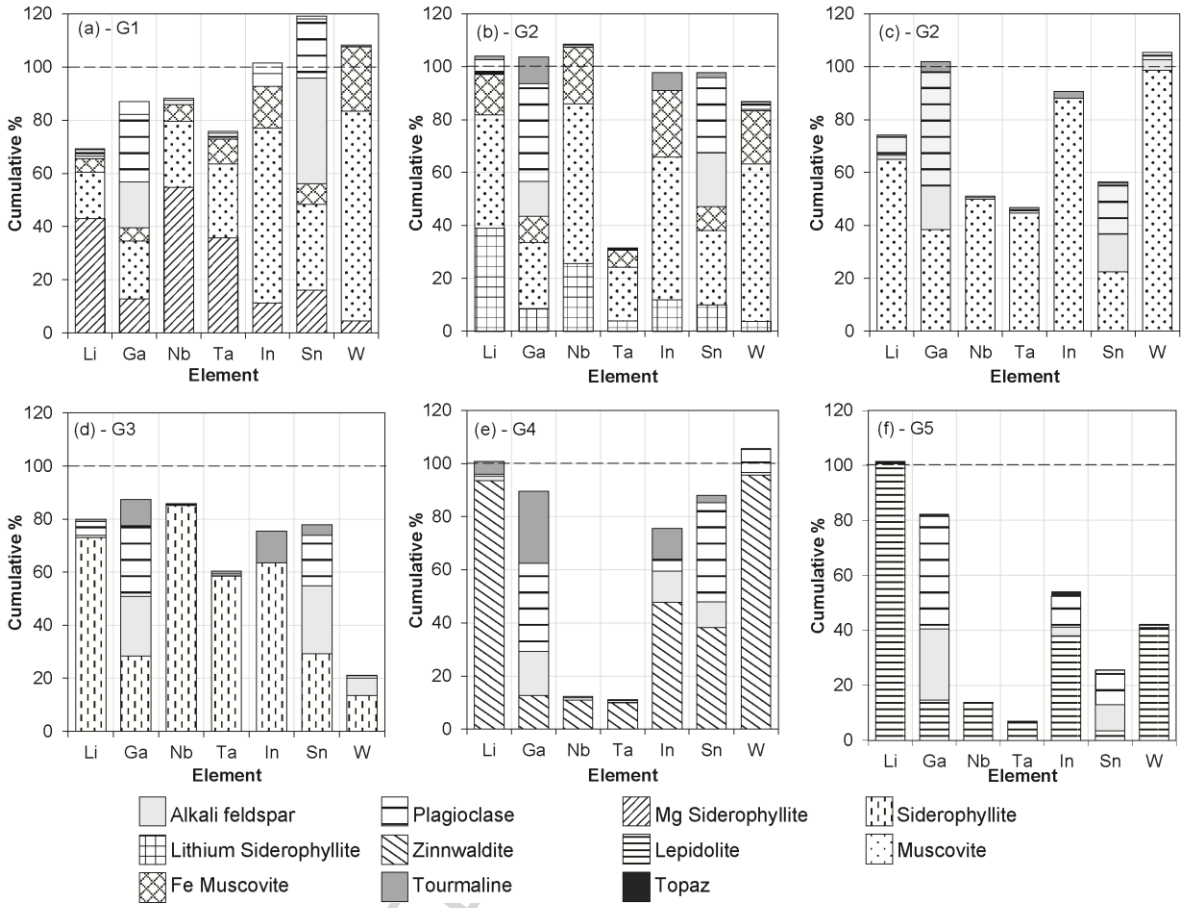

Figure 6

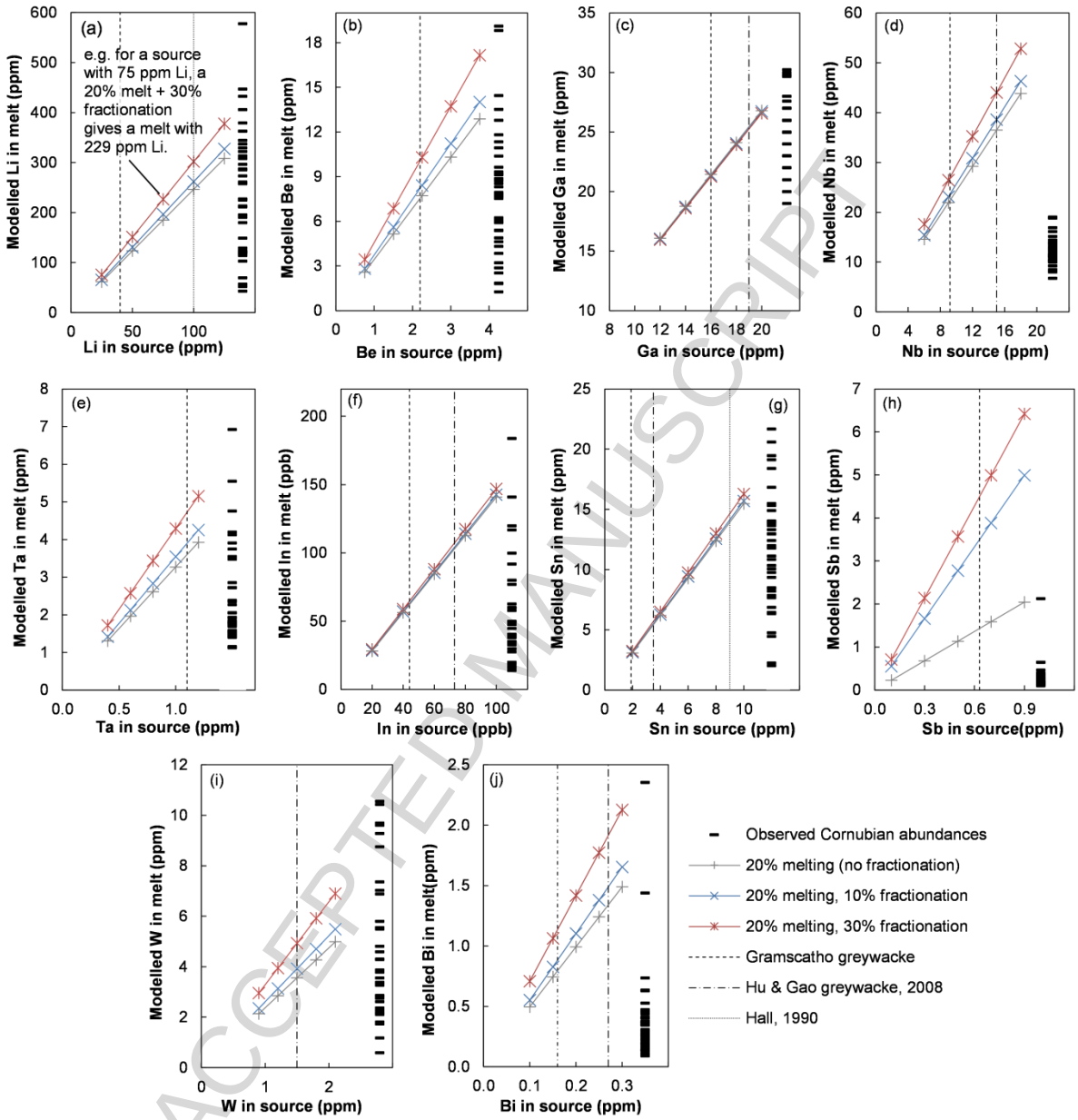

Figure 7

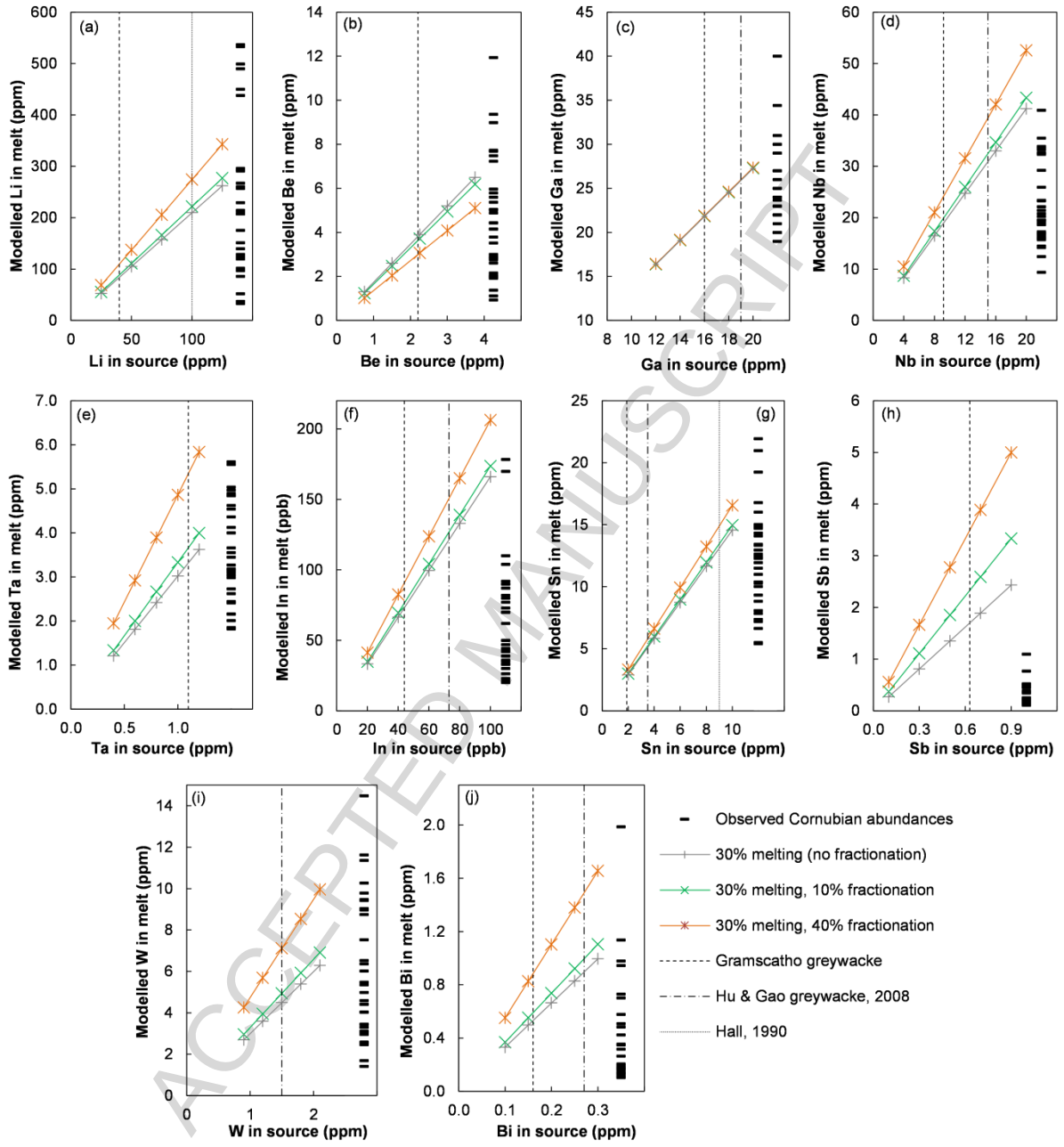

Figure 8

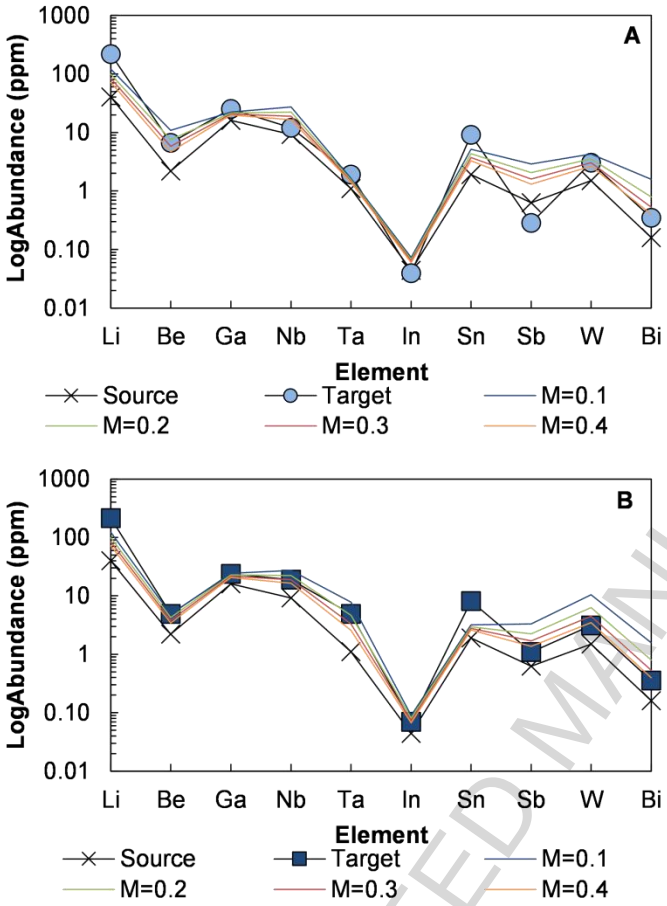

Figure 9

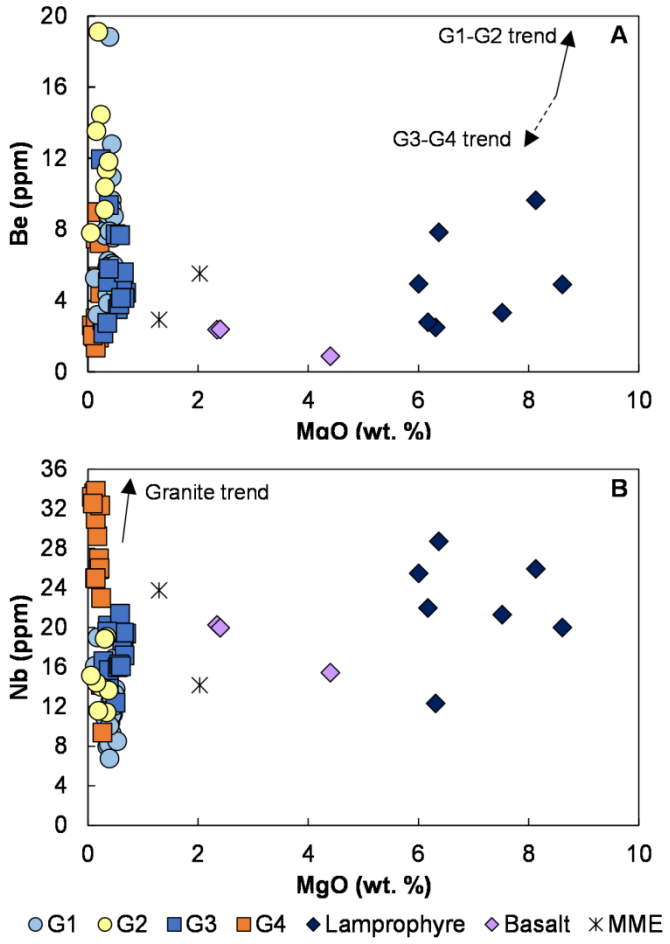

Figure 10

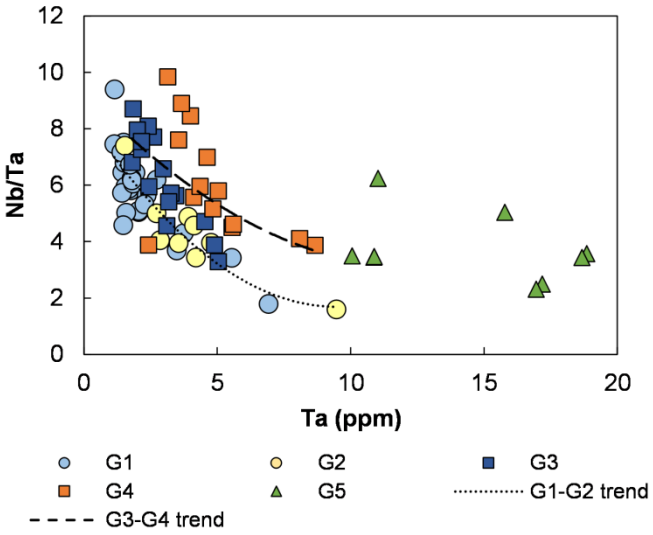

Figure 11

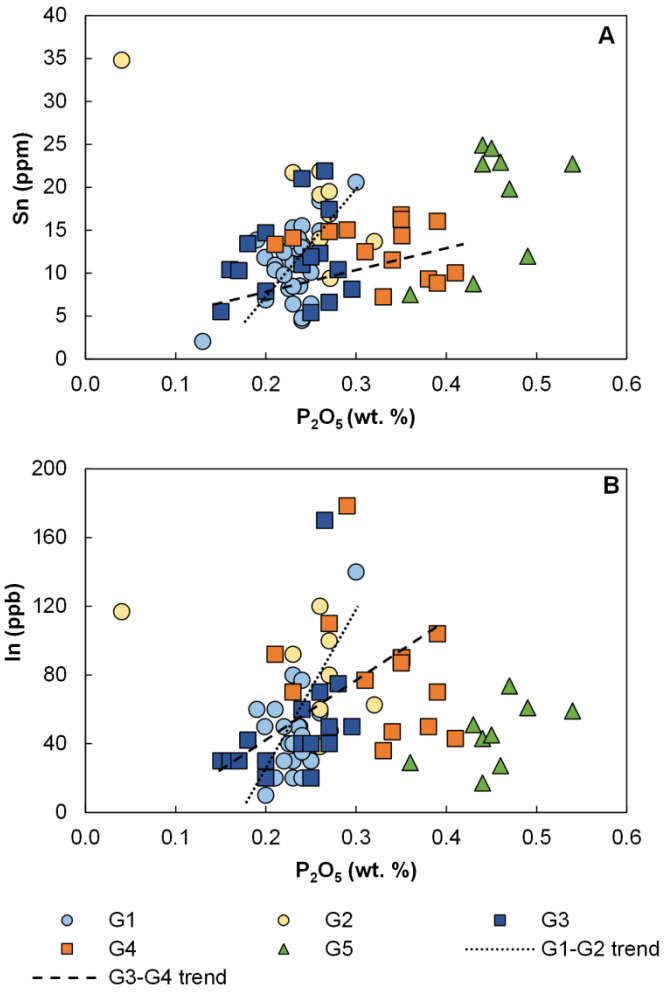

Figure 12

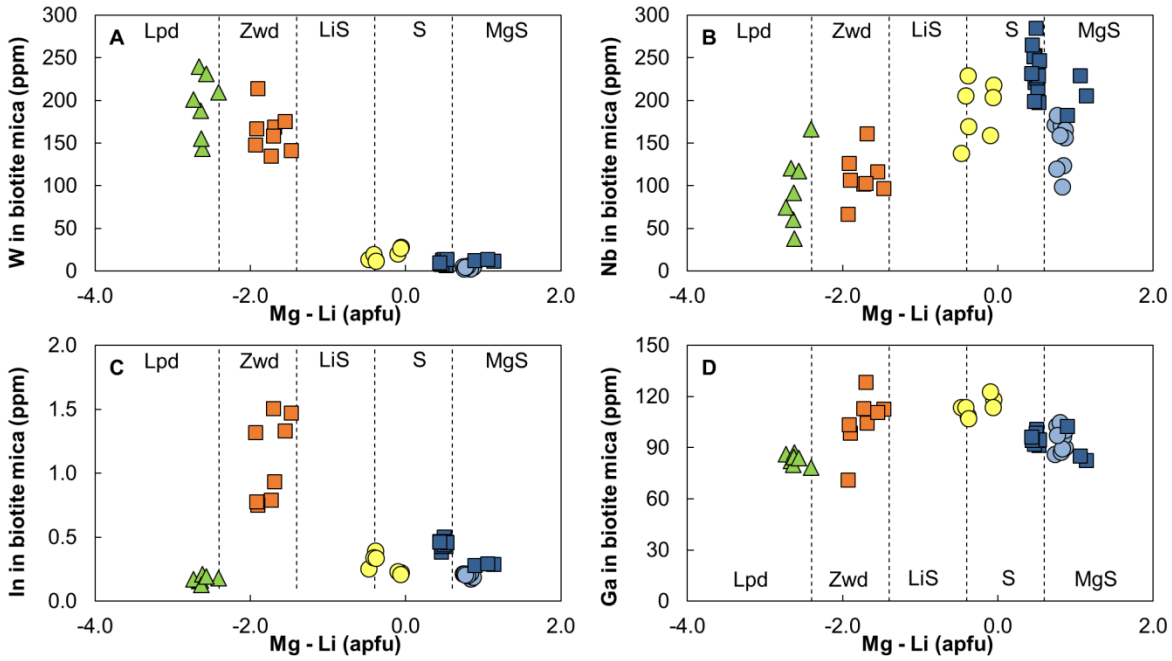

Figure 13

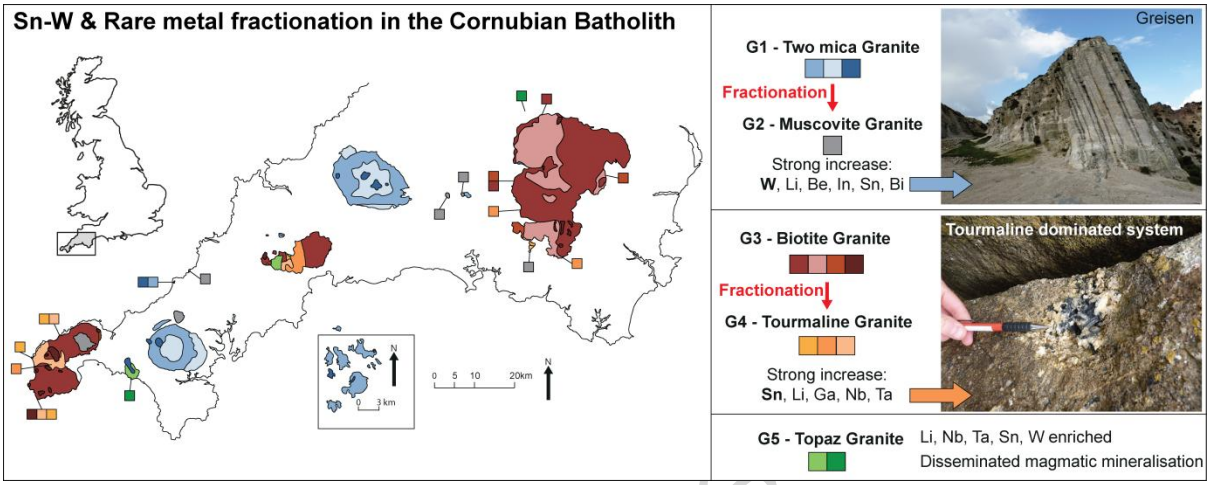

Graphical abstract

Highlights

- Fractionation of Li, Be, Ga, Nb, Ta, In, Sn, Sb, W and Bi in the G1-G5 granites of the Cornubian Batholith.
- New geochemical data for distribution of Ga, Nb, Ta, In, Sn and W in granite silicates.
- There is a strong W increase with fractionation from G1 to G2 granites. G2 are associated with greisen deposits.
- With fractionation from G3 to G4, there are strong increases in Li, Nb, Ta and Sn; accessory minerals host Nb and Ta in G4.
- G5 granites are enriched in Li, Ga, Nb, Ta, Sn and W, promoted by high F, and contain disseminated magmatic mineralisation.